Rewriting nuclear epigenetic scripts in mitochondrial diseases as a strategy for heteroplasmy control

Pérez, María J.[1,2]; Colombo, Rocío B.[1]; Real, Sebastián M.[1,3], Branham María T.[1,4] Laurito, Sergio R.[1,5], Moraes, Carlos T.[6], Mayorga Lía[1]

Affiliations:

1- Instituto de Histología y Embriología de Mendoza (IHEM, Universidad Nacional de Cuyo, CONICET). Mendoza, Argentina.
2- Facultad de Ciencias de la Nutrición. Universidad Juan Agustín Maza. Mendoza, Argentina.
3- Instituto de Fisiología, Facultad de Ciencias Médicas. Universidad Nacional de Cuyo. Mendoza, Argentina.
4- Facultad de Ciencias Médicas. Universidad de Mendoza. Mendoza, Argentina.
5- Facultad de Ciencias Exactas y Naturales. Universidad Nacional de Cuyo. Mendoza, Argentina.
6- Department of Neurology, University of Miami Miller School of Medicine. Miami, Florida, USA.

ABSTRACT

Mitochondrial diseases, caused by mutations in either nuclear or mitochondrial DNA (mtDNA), currently have limited treatment options. For mtDNA mutations, reducing mutant-to-wild-type mtDNA ratio (heteroplasmy shift) is a promising therapeutic option, though current approaches face significant challenges. Previous research has shown that severe mitochondrial dysfunction triggers an adaptive nuclear epigenetic response, characterized by changes in DNA methylation, which does not occur or is less important when mitochondrial impairment is subtle. Building on this, we hypothesized that targeting nuclear DNA methylation could selectively compromise cells with high levels of mutant mtDNA, favor ones with lower mutant load and thereby reduce overall heteroplasmy.

Using cybrid models harboring two disease-causing mtDNA mutations—m.13513G>A and m.8344A>G—at varying heteroplasmy levels, we discovered that both the mutation type and load distinctly shape the nuclear DNA methylome. We found this methylation pattern to be critical for the survival of high-heteroplasmy cells but not for the low-heteroplasmy ones. Consequently, by disrupting this epigenetic programming with FDA approved DNA methylation inhibitors we managed to selectively impact high-heteroplasmy cybrids and reduce heteroplasmy. These findings were validated in both cultured cells and an *in vivo* xenograft model.

Our study reveals a previously unrecognized role for nuclear DNA methylation in regulating cell survival in the context of mitochondrial heteroplasmy. This insight not only advances our understanding of mitochondrial-nuclear interactions but also introduces epigenetic modulation as a possible therapeutic avenue for mitochondrial diseases.

INTRODUCTION

Mitochondrial diseases impact approximately one in every 5,000 individuals, making them among the most prevalent inherited metabolic disorders [1–3]. To date, most of these disorders have inefficient or *no* treatment available. These diseases can arise from mutations in either nuclear or mitochondrial DNA (mtDNA). While traditional gene therapy approaches are becoming clinically available for nuclear genetic disorders [4–7],

manipulating the mitochondrial genome has proven more difficult due to its unique properties. mtDNA is small, circular, and exists in multiple copies within the mitochondrial matrix. It encodes for 13 essential respiratory chain subunits, 2 ribosomal RNAs and 22 transfer RNAs, necessary for mitochondrial translation. There are no known RNA import systems to the mitochondria [8,9], so base editing the mitochondrial genome has been challenging. However, new protein-only technologies have emerged for mtDNA editing[10,11]. Because mtDNA mutations co-exist with wild-type mtDNA (mtDNA heteroplasmy), the percentage of mutated molecules, defines the emergence of symptoms only when higher than a specific threshold[12]. Therefore, reducing the mutant to wild type mtDNA ratios or "heteroplasmy shift" is a valuable strategy for treatment. Although different techniques targeting the mtDNA for heteroplasmy shift have been successful in laboratory settings (mitochondrially targeted restriction endonucleases[13], zinc finger nucleases[14], mitoTALENs[15], mitoArcus[16]), none have *yet* reached clinical practice as gene therapy faces several challenges[17].

In this study, we propose a novel approach to lower heteroplasmy taking advantage of the natural communication between mitochondria and the nucleus, particularly the nuclear epigenome. Mitochondrial metabolites, such as succinate, fumarate, NAD, NADH and reactive oxygen species, modify the function of epigenetic enzymes (Jumonji C, TETs, DNA methyltransferases) [18–20]. Consequently, different degrees of mitochondrial stress modify nuclear transcriptomics[21], histone marks[22], and DNA methylation[23] in a specific manner. The latter has been proposed by us as an adaptive strategy to intense, chronic mitochondrial stress[23]. We previously showed that severe mitochondrial dysfunction triggered an epigenetic pro-survival response through modifications of the nuclear DNA (nDNA) methylation pattern, a phenomenon that did not occur when mitochondrial dysfunction was subtle[23]. Thus, considering that high-heteroplasmy is associated with severe mitochondrial respiration impairment, these cells may depend on an adaptive strategy which includes changes in nDNA methylation, a mechanism which would not be triggered in low-heteroplasmy cells. We hypothesized that manipulating the nDNA methylome would negatively impact the high-heteroplasmy cells, favor the prevalence of low heteroplasmy ones and consequently, reduce heteroplasmy (Fig 1). Notably, DNA methylation modulators like 5-Azacytidine and Decitabine are already FDA-approved for other conditions[24,25] raising the possibility of repurposing these drugs for mtDNA disorders.

Figure 1.

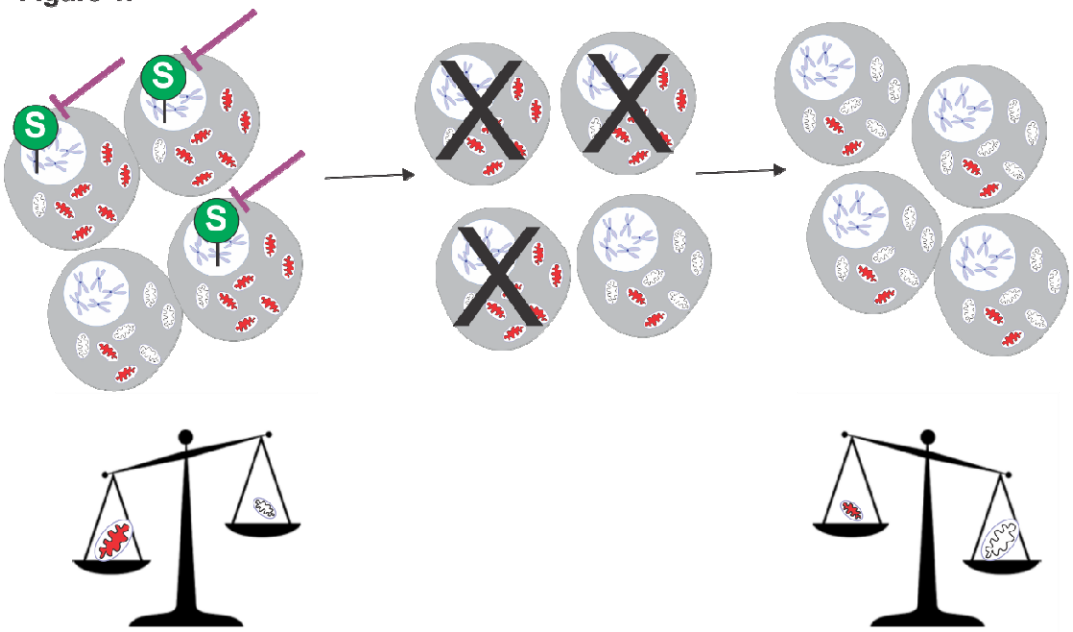

Figure 1. Working hypothesis. Mitochondrial dysfunction impacts the nuclear epigenome. Particularly, intense mitochondrial dysfunction determines a 'survival' nDNA methylation patterning[23]. Considering that high heteroplasmy implies intense mitochondrial impediment, these cells would have the 'S' nDNA methylation design whereas low heteroplasmy cells would not. By erasing this 'S' pattern, the survival of the high-heteroplasmy cells would be impaired favoring the low-heteroplasmy cells and therefore lowering heteroplasmy. Red mitochondria= mitochondria with mainly mutated mtDNA, white mitochondria= mitochondria with mainly wild-type mtDNA molecules. Green circle with a white 'S' represents a 'survival' nDNA methylation pattern.

METHODS

Mitochondrial disease model

Cybrids were obtained from the fusion of the osteosarcoma cell line143B.206 ρ0 mtDNA devoid cells with enucleated patient-derived dermal fibroblasts as previously described[26,27]. We used cybrids harboring wild-type mtDNA and two disease causing mutations: m.13513G>A (MT-ND5) [28–30] and m.8344A>G (MT-tRNA-Lys)[31,32]. Clones with different levels of heteroplasmy were obtained by treating cybrids with Ethidium Bromide (50ng/ml - 2 weeks) to partially deplete them from mtDNA followed by cell dilution, clone selection and random mtDNA repopulation[26] in Ethidium Bromide free medium. High (above the usual disease triggering threshold) and low (below the threshold) heteroplasmy clones were selected for further experiments. The clones were abbreviated as 13H (cybrids harboring ≥70% m.13513G>A mutation), 13L (≤30% m.13513G>A mutation), 8H (≥95% m.8344A>G mutation), 8L (<50% m.8344A>G mutation, although for cell culture experiments 8L with <5% heteroplasmy were used).

For a few additional experiments, we also used embryonic fibroblasts (MEFs) derived from a heteroplasmic mouse model carrying the mtDNA tRNA-Ala m.5024C>T mutation[33] which were immortalized with the E6-E7 gene from the human papilloma virus (HPV)[34] and human dermal fibroblasts containing the m.14459G>A MT-ND6 mutation (also immortalized with the HPV E6-E7 gene).

Cells were grown at 37ºC, 5% CO_2, in DMEM high-glucose (Gibco®, cat#11995065), supplemented with 10% fetal bovine serum (Gibco®, cat#16000044), 100U/ml

Penicilin+ Streptomicine (Gibco®, cat#15140122) and uridine (Sigma-Aldrich ®U3003) 50µg/ml.

DNA extraction

CTAB/chloroform-isoamylic based protocol. Cells were collected and tissues were homogeneized in PBS using an Ultra turrax homogenizer, following centrifugation, the pellet (cells or tissue) was suspended and washed 1 time with Tris–EDTA ($T_{10}E_{10}$), suspended in cetyltrimethylammonium bromide (CTAB) solution (2 g/l CTAB Sigma-Aldrich®, 100 mM Tris/HCl, 20 mM EDTA and 2% 2-mercaptoethanol) and incubated at 60 °C for 1 h for cells or overnight for tissue. Then, chloroform-isoamyl alcohol solution (24:1) was added and the sample was centrifuged. The aqueous phase was collected into a new tube and mixed with 3 volumes of ice-cold 100% ethanol. Precipitated DNA was dissolved in $T_{10}E_{0.1}$.

Alternatively, when few cells were available, DNA was purified using the DNA PuriPrep-S kit (Inbio Highway®, cat#K1205-50), following manufacturer´s protocol.

Heteroplasmy and mtDNA content assessment (SYBR based qPCR)

qPCR was carried out using SsoAdv univer SYBR GRN BioRad® (cat#1725271). 1ng of total DNA was used for each PCR reaction. Aria Mx-Real time PCR system/Agylent technologies®) was used to readout the PCRs.

mtDNA mutation heteroplasmy was measured using 3 primers for each mutation: one forward primer (F) and two reverse primers: one specific for the mutated version (R-mut) and the other a few base pairs downstream to the mutation with the ability to amplify both mutated and wild-type molecules (R-all). Heteroplasmy was quantified using ΔCT method= $2^{-(mutCT-allCT)}$.

mtDNA content was estimated by normalizing the mtDNA ´all´ amplicon to the one of a nuclear gene (B2M), quantified using ΔCT method= $2^{-(allCT-B2MCT)}$.

Primers

Mutation or gene	strand	Sequence 5´-3´
m.13513G>A (homo sapiens)	F	GGGTCCATCATCCACAACCTT
	R-mut	GCGGTTTCGATGATGTGGTT
	R-all	TTGCGGTTTCGATGATGTGG
m.8344A>G (homo sapiens)	F	AAACCACAGTTTCATGCCC
	R-mut	CACTGTAAAGAGGTGTTGGC
	R-all	TTCACTGTAAAGAGGTGTTGG
B2M (homo sapiens)	F	GACTTGTCTTTCAGCAAGGA
	R	ACAAAGTCACATGGTTCACA
m.5024C>T (mus musculus)	F	AGCTATCATAAGCACAATAACCC
	R-mut	AATAGATGTAGGATGAAGTCTTACGA
	R-all	CAATAGATGTAGGATGAAGTCTTACA

qPCR conditions

Mutation or gene	amplicon	Primer concentration (F and R)	Thermal cycling conditions
m.13513G>A	13-mut	0.25µM	Start: 95ºC 3' Cycling (x40):

	13-all	0.25µM	95ºC 15" 60ºC 30" (reading) 72 ºC 30"
m.8344A>G	8-mut	0.25µM	Start: 95ºC 3' Cycling (x40): 95ºC 15" 60ºC 30" (reading) 72 ºC 30"
	8-all	0.5µM	
B2M	B2M	0.25 µM	Start: 95ºC 3' Cycling (x40): 95ºC 15" 60ºC 30" (reading) 72 ºC 30"
m.5024C>T	5024-mut	0.15 µM	Start: 95ºC 3' Cycling (x40): 95ºC 15" 58ºC 30" (reading) 72 ºC 30"
	5024-all	0.5 µM	

DNA methylation studies

Methyl specific multiplex ligation dependent probe amplification (MS-MLPA)[35]

The ME001-C2 or D1 and ME002-C2 kits (MRC-Holland®) were utilized for the assays. The MS-MLPA process involved the following steps: 50 to 100 ng of total DNA was used to initiate the reaction, following adding probes which hybridized for 18 hours at 60 °C. Subsequently, ligation was carried out at 54 °C, and the reaction mixture was split into two halves. One half was digested at 37 °C for 30 minutes with the methyl-sensitive restriction enzyme CfoI, which specifically cleaves unmethylated 5′-GCGC-3′ sequences, while the other half was left undigested to serve as a reference. Both ligated samples were then amplified via PCR using FAM-labeled MLPA primers. The resulting fluorescent-labeled PCR products were analyzed by capillary electrophoresis on an ABI-3130 sequencer (Applied Biosystems®) and further processed with GeneMarker v1.75 software (Softgenetics®). The mean methylation value for each CpG site from each condition was used for hierarchical clustering and heat map confection.

Methylation analysis using Infinium EPIC 850k chips[36] *(Supplementary file 1)*

~500ng genomic DNA (from 14 samples: two wild-type, three 13H, three 13L, three 8H, three 8L samples) was submitted to bisulfite conversion using the EZ DNA Methylation – GoldTM kit (ZymoResearch®). Bisulfite converted DNA was thereafter hybridized to the Illumina Infinium Methylation EPIC BeadChip, representing the methylation state of over 850,000 CpG sites. The array was imaged using the Illumina iScan system (Illumina®). GenomeStudio® software was used for processing. Steps as follows, Quality check → Background Correction & Dye Bias Equalization → Filtering → BMIQ Normalization → Data Transformation. Each methylation data point is represented by fluorescent signals from the M (methylated) and U (unmethylated) alleles. Background intensity computed from a set of negative controls was subtracted from each analytical data point. The ratio of fluorescent signals was then computed from the two alleles Beta value = (max(M, 0))/(|U| + |M| + 100). The Beta-value reflects the methylation level of each CpG site. A Beta-value of 0-1 was reported signifying percent methylation,

from 0% to 100%, respectively. To calculate differential methylation for each CpG site, we used the following formula:
Δ (delta) = mean(Avg_beta of Test group) - mean(Avg_beta of Control group). We performed
Mutated vs. wild-type and high vs. low heteroplasmy comparisons.
Beta values from each site and sample are available in Supplementary file 1.
Identification of significant differentially methylated CpG sites:
CpG sites were considered hypermethylated if $\Delta \geq 0.2$, and hypomethylated if $\Delta \leq -0.2$.
Additionally, significance required a p-value < 0.05 from a one-tailed, unpaired Student's t-test, and the differential methylation needed to occur towards the same direction (hyper or hypo) in two or more consecutive CpG sites in the genome (based on the Infinium MethylationEPIC v1.0 B5 Manifest File).
From these CpG sites, we selected the ones associated to particular genes and that list was imported to the Metascape online tool (http://metascape.org)[37] to perform "custom" analysis, searching for enrichment of genes under membership categories in any pathway that involved the term *survival* (in pathway name or description).
Regarding ESR1 associated CpG sites we ploted their beta values using GViz R package v1.46.1 and dependencies. The scripts used for data processing are available in our GitHub repository https://github.com/slaurito/Methylation-Analysis-from-Nanopore-and-Epic-Data-Perez-et-al.

Methylation analysis and mtDNA sequencing using (MinION) Oxford Nanopore Technologies® [38](Supplementary file 2)

~200 ng DNA samples from xenograft tumors conditions (13H, 13H-dec, 13L and 13L-dec, three tumors from each condition, total of 12 samples) were used as input for Nanopore sequencing. The library was prepared using the Rapid Barcoding Kit from Oxford Nanopore Technologies, following the manufacturer's instructions. Briefly, this system employs transposome complexes that cleave the DNA and add barcodes to each sample. The samples are then pooled, and the library is purified using magnetic beads. Finally, sequencing-specific adapters are added. Sequencing was performed on a MinION Mk1C device for 48 hours at 37ºC, generating POD5 files for subsequent analysis. POD5 files were processed for base calling using Dorado basecaller v0.9.1, including the identification of 5-methylcytosine and 5-hydroxymethylcytosine using the high-accuracy model (HAC). The resulting .BAM files were aligned to the reference genome Hg38, obtained from the UCSC Genome Browser (https://genome.ucsc.edu/), using Dorado aligner. Subsequently, the .BAM files were sorted and indexed using SamTools. Additionally, for further analyses, .bedmethyl files containing the genomic coordinates of all modified cytosines were obtained using ModKit v0.4.4.For the bioinformatics analysis, the NanoMethViz[39] v2.8.1 package was initially used to generate a Tabix file (Supplementary file 3) containing the chromosomal coordinates of each detected cytosine modification and its Log-Likelihood Ratio (LLR), which indicates the probability of cytosine modification. The functions NanoMethResult() and plot_region() were employed to generate heatmaps and visualize methylation levels across the mitochondrial genome. For global methylation analysis at the chromosomal and total genome levels, the methy_to_bsseq() and bsseq_to_log_methy_ratio() functions were used to convert the LLR of each genomic position into a logarithmic methylation ratio (LMR). Prior to statistical analysis and plot generation, the log-methylation ratios were transformed into values ranging from 0 (unmethylated) to 1 (methylated) using a sigmoidal function: $1/1+e^{-LMR}$. Statistical analyses were performed using the Shapiro-Wilk test for normality assessment and then Wilcoxon test.

For the analysis of the mitochondrial genome mutation 13513 G>A, Rsamtools v2.18.0 was used. Heteroplasmy was calculated as ´A´ counts/(´A´counts+´G´ counts).
The scripts used for data processing are available in our GitHub repository https://github.com/slaurito/Methylation-Analysis-from-Nanopore-and-Epic-Data-Perez-et-al.

DNA methylation modulation treatments in cell culture

DNA methylation inhibition through drugs:
Equal amounts of cybrid cells were plated (separately or in a 1:1 high:low heteroplasmy mixture) to a 70% confluency for 1-day treatments or to a 50% confluency for 3-day treatments. 24h afterwards, 5-azacytidine (Sigma-Aldrich®, cat#A2385) or 5-aza-2′-deoxycytidine= decitabine (Merck-Millipore® cat#189826) was added at different concentrations, i.e., 0.1 µM, 1 µM and 10 µM. Equal amounts of their vehicle (DMSO, Merck-Millipore®) were used for control conditions. For 3-day treatments, drugs were replenished every 24h.
DNA methylation inhibition through IPTG-Inducible shRNA DNMT1 knockdown lentiviral vector. Generation of a stable cell line of m.13513G>A low and high-heteroplasmy cybrids with the mammalian pLV[shRNA]-LacI: T2A:Puro-U6/2xLacO>hDNMT1[shRNA#1] purchased in Vector Builder®. Lentivirus were produced in Hek293T cells by transient co-transfection of the MISSION® Lentiviral Packaging Mix(Sigma®) with 1.35 µg of the shRNA-encoding DNA using 7 µg polyethylenimine(PEI, Poliscience®) for transfection of a well from a 6-well plate. Culture supernatants were collected 48 and 72 h post transfection, filtered (0.22 mm filter, cellulose acetate, Ministart®), and supplemented with 8 µg/ml polybrene (Sigma®). Subconfluent cybrids (~70%) in a well from a 6-well plate were infected with the polybrene-supplemented supernatant and 48 h post-infection were selected with 1 µg/ml puromycin (sc-108071®) for 1 week. These cybrids were treated with IPTG: isopropyl-galactosidase (TRANS®) 500 µM for 72 h (replacing medium and IPTG every day) and DNMT1 down-regulation was checked through Western Blot (Fig S2).

Proliferation assays
We used Cell Proliferation Assay Kit (BN00566_ Assay Genie®): ~3000 cells/well were plated in a 96-well plate before treatment with demethylating agents. 24h afterwards, basal cell density was measured with fluorometer (Fluoroskan™ Thermo Scientific™ microplate reader) after following proliferation assay´s protocol and treatments with drugs were started. At day 3 proliferation assay and fluorescence measurement were repeated as in the basal condition. For quantification, fluorescence after 3-day treatment was relativized to basal fluorescence before treatments.

Mitochondrial membrane potential analysis
Tetramethylrhodamine ethyl ester, perchlorate (TMRE) (Molecular probes®) was used. Cells were incubated with 50nM TMRE at 37 ºC in culture medium in the dark for 30 min; cells were then taken up and passed through flow cytometer (FACSAria flow cytometer_BD®). The fluorescence was evaluated using excitation at 488 nm and read with band pass filter 585/42 nm. As a positive depolarization control, cells were treated with 100 µM Carbonyl cyanide m-chlorophenyl hydrazone (CCCP, Sigma-Aldrich®) concomitantly with TMRE. Results were analyzed with FlowJo v X.0.7® software.

Apoptosis assays

Annexin V-FITC (BD-Biosciences®) was used to measure apoptosis. Cells were taken up at the end of treatments and ~ 50,000 cells/condition were used. They were centrifuged, washed and then resuspended in 50 µl AnnexinV buffer (10 mM HEPES, 140 mM NaCl, 2.5 mM CaCl2, pH 7.4) + 2 µl AnnexinV-FITC. The samples were incubated in the dark at room temperature for 15 min and then 200 µl of ice cold Annexin buffer was added (250 µl final volume). Fluorescence was evaluated through flow cytometry (FACSAria flow cytometer_BD®) using excitation 488 nm, emission 530/30 nm. Flow cytometry assays were analyzed using FlowJo v X.0.7® software.

Western Blots

Cells were lysed with lysis buffer solution (TRITON 0.5%, NaCl 150 mM, EDTA 5 mM, Tris–HCl 1 M, pH 7.5 + Halt™ protease inhibitor cocktail) and proteins (20 µg, measured with Pierce™ BCA Protein Assay Kit, Thermofisher Scientific®) were run on a 10% (DNMT1 and ESR1) or gradient 4-20% (TGX Stain-free gels Cat # 456-8096, for OXPHOS rodent WB antibody cocktail) SDS–polyacrylamide gel and then transferred to a nitrocellulose membrane. The membranes were blocked in 5% lowfat milk-PBS solution and then incubated overnight at 4 °C with primary antibodies: anti-DNMT1:1000 (rabbit-antibodies.com®- cat#A307589), anti-ESR1 1:1500 (rabbit-CSB-PA11399A0Rb Cusabio®), total OXPHOS rodent WB antibody cocktail 1:1000 (mouse-ab110413- abcam®), anti-β-actin 1:5000 (mouse- Invitrogen® cat# MA1-149) anti-vinculin 1:5000 (mouse- Sigma-Aldrich®) followed by PBS-Tween washes and secondary antibody incubation (1.5 h at room temperature): mouse (Gt anti-mouse IgG -H + L -Invitrogen®) 1:10,000 and rabbit (Gt anti-Rb IgG -H + L- Invitrogen®) 1:3000. Bands were developed using chemiluminescence (ECL BPSBioscience®), visualized with a LAS Fujifilm 4000 system (GE Healthcare Life Sciences®) and quantified using Image J® software.

Oxygen consumption rate (OCR)

OCR was measured using a Seahorse XFp Extracellular Flux Analyzer (Seahorse Bioscience®). 2 days prior to the assay, cells were seeded at a density of 30,000 cells/well in wells B-G (wells A and H contained media only). 24h afterwards DMSO or decitabine were added in triplicate conditions to a concentration of 1µM. The XFp sensor cartridge was calibrated with calibration buffer overnight at 37 °C. The following day, cell culture medium was replaced with buffered Seahorse medium supplemented with glucose, pyruvate, and glutamine to reach same concentration as DMEM high glucose, and incubated for at least 1 h at 37 °C. Mito-stress test[40] was carried out and measurements of endogenous respiration were measured following sequential addition of 5 µM Oligomycin, 1 µM Trifluoromethoxy carbonylcyanide phenylhydrazone (FCCP), and 5 µM Rotenone plus Antimycin A 2.5 µM. Results were normalized to µg protein per well after the Seahorse run, protein was quantified using Lowry Method Bio-Rad® Detergent Compatible (DC) Protein Assay. Alternatively, results were normalized to cell number by BioRad® TC20 Automated Cell Counter.

Reactive oxygen species (ROS) measurement

2′,7′-Dichlorofluorescin diacetate (DCF-DA) (Sigma- Aldrich®) was used. The different conditions were loaded with the probe in cell medium at a 10 µM concentration and incubated at 37 °C for 30 min in the dark. Then, cells were taken up, rinsed with PBS and passed through flow cytometer (FACSAria flow cytometer_BD®), excitation: 488 nm; band pass filter 530/30 nm.

Cell tracking

m.13513G>A low-heteroplasmy cybrids (13L) were labelled with Green CMFDA (5-Chloromethylfluorescein Diacetate, ab145459, abcam®) 10µM at 37 °C for 45 min in the dark. Afterwards, these dyed cells and undyed m.13513G>A high-heteroplasmy cybrids (13H) were taken up and counted using BioRad® TC20 Automated Cell Counter. Equal amounts were mixed and plated before treatments. 24h later, treatment with DMSO, 5-azacytidine and decitabine were initiated. After the 3-day treatment, cells were taken up and the % of FITC(+) cells was measured through flow cytometry (FACSAria flow cytometer_BD®), excitation: 488 nm; band pass filter 530/30 nm.

Indirect immunofluorescence

Mitophagy evaluation assays

Cells were fixed with 4 % Paraformaldehyde solution 30 min at room temperature, following washes with PBS, and then quenched with $ClNH_4$ 50 mM for 30 min at room temperature. Cells were then permeabilized with Albumin 2 %/Saponin0.1 % PBS solution, following which they were incubated with anti-MAP1 LC3B 1:200 (A7198, antibodies.com® rabbit) and mouse anti-human TOMM20 antibody 1:200 (clone AT1B2 LS-C755581) overnight at 4 ºC. The primary antibodies were rinsed and then cells were

incubated with secondary antibodies ab150077 Goat Anti-Rabbit IgG H&L (Alexa Fluor® 488) 1:750 and ab150115 Goat Anti-Mouse IgG H&L (Alexa Fluor® 647) 1:750, washed, and coverslips were mounted on glass slides using Mowiol + Hoechst 34580 1:1000 (Thermo Scientific®, cat#62249) and examined by fluorescence confocal microscopy (Olympus Confocal Microscope FV1000-EVA®).

Xenografts.

Ten six-week-old female NSG mice (~25 g) were anesthetized with isofluorane 4% in O_2, and injected subcutaneously in their backs with m.13513G>A cybrids (suspended in PBS) to generate 3 subcutaneous tumors in each mouse. 10^6 high-heteroplasmy (13H), 10^6 low heteroplasmy (13L) and 10^6 mixed heteroplasmy (half high 13H and half low 13L) cybrids were implanted separately and distinctively in the back of each mouse. We decided to inject the 3 types of cells in each mouse to reduce inter-animal differences and to optimize the number of animals used for the experiment. When all tumors became palpable (13 days after injection) half the mice were selected for the control group and half for the treatment one. The experimental mice were treated with intraperitoneal decitabine 1mg/kg dissolved in PBS every other day for 8 days (4 doses were applied). The controls were treated with the equivalent vehicle (DMSO in PBS). Mice were closely monitored, and tumor size was measured every other day. Tumor volume was calculated as= length*width^2/2/1000. The mice were then euthanized in a CO_2 chamber, and tumors were excised. To obtain a reliable heteroplasmy value, representative to the whole tumor, tumors were homogenized in PBS with an Ultra turrax homogenizer and DNA was extracted from the resulting tissue pellet. (sketch in Fig 8A)

The highly immunosuppressed Nod Scid Gamma (NSG) mice (NOD.Cg-PrkdcscidIl2rgtm1Wjl/SzJ, NSG) (RRID:IMSR_JAX:005557) used in these experiments were obtained from Jackson Laboratory and were housed in a pathogen-free condition throughout the experimental duration. All procedures were performed following the consideration of animal welfare and were approved by the Institutional Committee for Care and Procedures of Laboratory Animals (CICUAL in Spanish) of the National University of Cuyo, Mendoza, Argentina. All procedures were approved by the Institutional Animal Care and Use Committee of the School of Medical Science,

Universidad Nacional de Cuyo (Protocol approval N° 192/2021). All animals were cared for in accordance with the guiding principles in the care and use of animals of the US National Institute of Health.

Statistics software

Graph Pad Prism v5.03® was used for most statistical analyses and graph confection.
EPIC studies required GenomeStudio Software® ans ggplot2, tidyr y ggpubr R packages.

Art work

Corel draw 2021® was used to draft figures.
MS-MLPA heatmap (Fig 2A) was done using Complex Heatmap R package.
Violin plots and box plots in Fig 3B were prepared with ggplot2, tidyr y ggpubr R packages.
EPIC heatmap (Fig 3C) was prepared with heatmapper.ca[41].
Fig 8 contains images modified from Biorender®.

Article drafting

We used ChatGPT, an AI-powered language model developed by OpenAI, solely for language-related assistance in the composition of this research paper, with no influence on the content or research outcomes.

RESULTS

As a model of mitochondrial diseases, we used transmitochondrial cybrids [26,27] harboring wild-type mtDNA and two disease causing mutations: m.13513G>A (MT-ND5) [28–30] and m.8344A>G (MT-tRNA-Lys)[31,32]. The ND5 mutation is associated with Leigh syndrome[42], MELAS[43] and LHON[44] phenotypes. The m.8344A>G mutation is most often associated with the MERRF[31,45] phenotype. Cell clones with high or low mtDNA mutant loads, based on previously defined phenotypic thresholds or severities[46–48], (see methods for specific heteroplasmies) were selected for further experiments. For brevity, we refer to cybrids harboring the m.13513G>A mtDNA mutation As “13” followed by “L” for low mutant load and “H” for high mutant load. Likewise, the m.8344A>G cybrids are referred to as 8L and 8H. The distinct mitochondrial functioning between high and low-heteroplasmy cybrids was validated through differences in mitochondrial membrane potential (Fig S1).

The nuclear DNA methylome is shaped by both the degree of mtDNA heteroplasmy and the nature of the mtDNA mutation.

DNA methylation of Tumor suppressor genes

Since our hypothesis states that DNA methylation could be important for the survival of high-heteroplasmy cells, we analyzed the methylation status of CpG sites located in promoter regions from tumor suppressor genes that are commonly hypermethylated in cancer (paradigm of cellular survival) [49–51]. We investigated 52 CpG sites using MS-MLPA (Methyl-specific multiple ligation-dependent probe amplification)[35] in promoter regions of 35 tumor suppressor genes in wild-type and mutated cybrids.

Unsupervised hierarchical cluster using Manhattan’s distance and average linkage clustering method of the mean methylation percentages of each group was performed to demonstrate differences or similarities between the groups (Fig 2A). When

comparing paired CpG by CpG mean methylation levels, there was a greater methylation of these regions in the 13H cybrids compared to the 13L and wild-type ones (Fig 2B). This is in accordance with our previous work, in which we had observed an increased methylation of these sites (plus others) in samples coming from mitochondrial disease patients[23]. The ´8´ cybrids did not differ between the high and low-heteroplasmy group regarding these regions but did exhibit a generalized lower methylation level compared to the ´13´ cybrids (Fig 2B). Therefore, at least for the ´13´ mutants, in line with our hypothesis, as heteroplasmy levels increase, CpGs related to tumor suppressor genes show greater methylation, which in theory, would enhance the survival capacity of the high-heteroplasmy cells.

Additionally, we tested different strategies to reduce DNA methylation levels globally. For this, we treated 13H cells with DNA methylation inhibitors: 5-azacytidine and decitabine. Furthermore, we knocked down the expression of the DNA methyltransferase 1 (DNMT1, knockdown control in Fig S2), necessary for maintaining the DNA methylation pattern[52]. All three approaches decreased the methylation status of these CpG sites with decitabine being the most effective to do so (Fig 2B).

Figure 2.

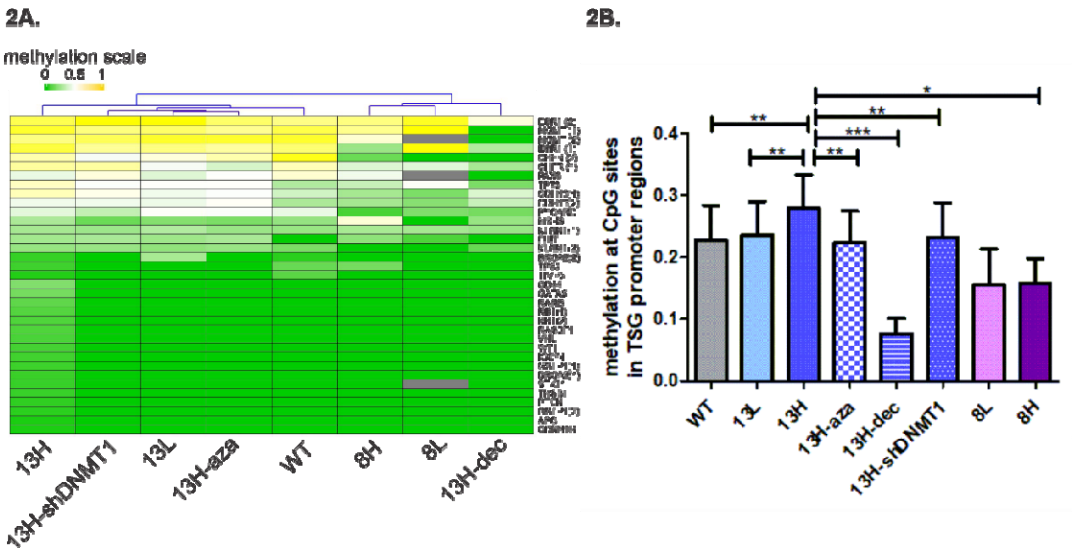

Figure 2. DNA methylation of CpG sites in promoter regions of tumor suppressor genes (TSG) differs between groups. 2A. Heat map and hierarchical cluster of CpG sites in cybrid samples using Manhattan's distance and average linkage clustering method of the mean methylation percentages of each group. Color scale: green, methylation=0%, yellow, methylation=100% (1), white, methylation= 50% (0.5). grey= not analyzed: N/A. Column cluster dendrogram is shown, row clustering was performed but dendogram is not shown. **2B.** Comparison of the mean methylation level of TSG promoter regions. Paired CpG-by-CpG comparison (mean methylation of each CpG site from the different sample groups was used for the one-tailed paired Student's t-test).***p<0.001, **p<0.01, *p<0.05. WT= wild-type cybrids, 13L= low-heteroplasmy m.13513G>A cybrids, 13H= high-heteroplasmy m.13513G>A cybrids, aza= 5-azacytidine, dec= decitabine, shDNMT1= IPTG-Inducible shRNA DNMT1 knockdown. N= ≥2 samples per condition.

Genome-wide methylation

Given the changes observed in a limited number of CpG sites, we expanded our analysis to investigate global DNA methylation. Using Illumina's Infinium EPIC 850k

array[36], which covers over 850,000 CpG sites across the genome, we examined genome-wide methylation patterns of wild-type, 13H, 13L, 8H and 8L cybrids.

Unsupervised hierarchical clustering of these methylation profiles (using Manhattan's distance and average linkage) revealed that the samples clustered according to mutation type and load. This suggests that both the form and intensity of mitochondrial dysfunction are key determinants of the DNA methylation profile (Fig. 3A).

Mean beta values (which represent the methylation level at each CpG site)[36] across the genome exhibited increased levels of DNA methylation in high-heteroplasmy cells (Fig 3B, left panel), in accordance with our previous work with patients´ muscle samples [23], and with the methylation level of tumor suppressor genes described above. Additionally, the ´13´ mutant cybrids globally showed higher methylation than the ´8´ lines, and higher than the wild-type cells (Fig 3B, right panel), again in line with what we had observed in tumor suppressor genes. Importantly, the differentially methylated CpG sites followed the same global methylation trend. When comparing mutant versus wild-type cybrids (Fig. 3C, left panel), most differentially methylated sites were hypermethylated, and the same pattern was observed when comparing high- versus low-heteroplasmy cybrids (Fig. 3C, right panel). Sample 8L_1, with a borderline heteroplasmy level (~50%), exhibited a closer association with the high-mutant samples. Beta-values for each site and sample are available in Supplementary file 1.

While the implications of nuclear DNA methylation are well-established[53–56], the extent, nature, and significance of mtDNA methylation remain controversial[57,58]. Given our focus on mtDNA mutations and mitochondrial dysfunction, we did not forget to look at mtDNA methylation. Despite its underrepresentation in the EPIC array (with only 7 probes among over 850,000), none of these mtDNA CpG sites showed differential methylation in any of our comparisons (mutant vs. wild-type, high vs. low heteroplasmy, mutant 13 vs. mutant 8; Supplementary file 1). This suggests that the significant differential methylation profile we observed is driven by nuclear DNA changes.

Figure 3.

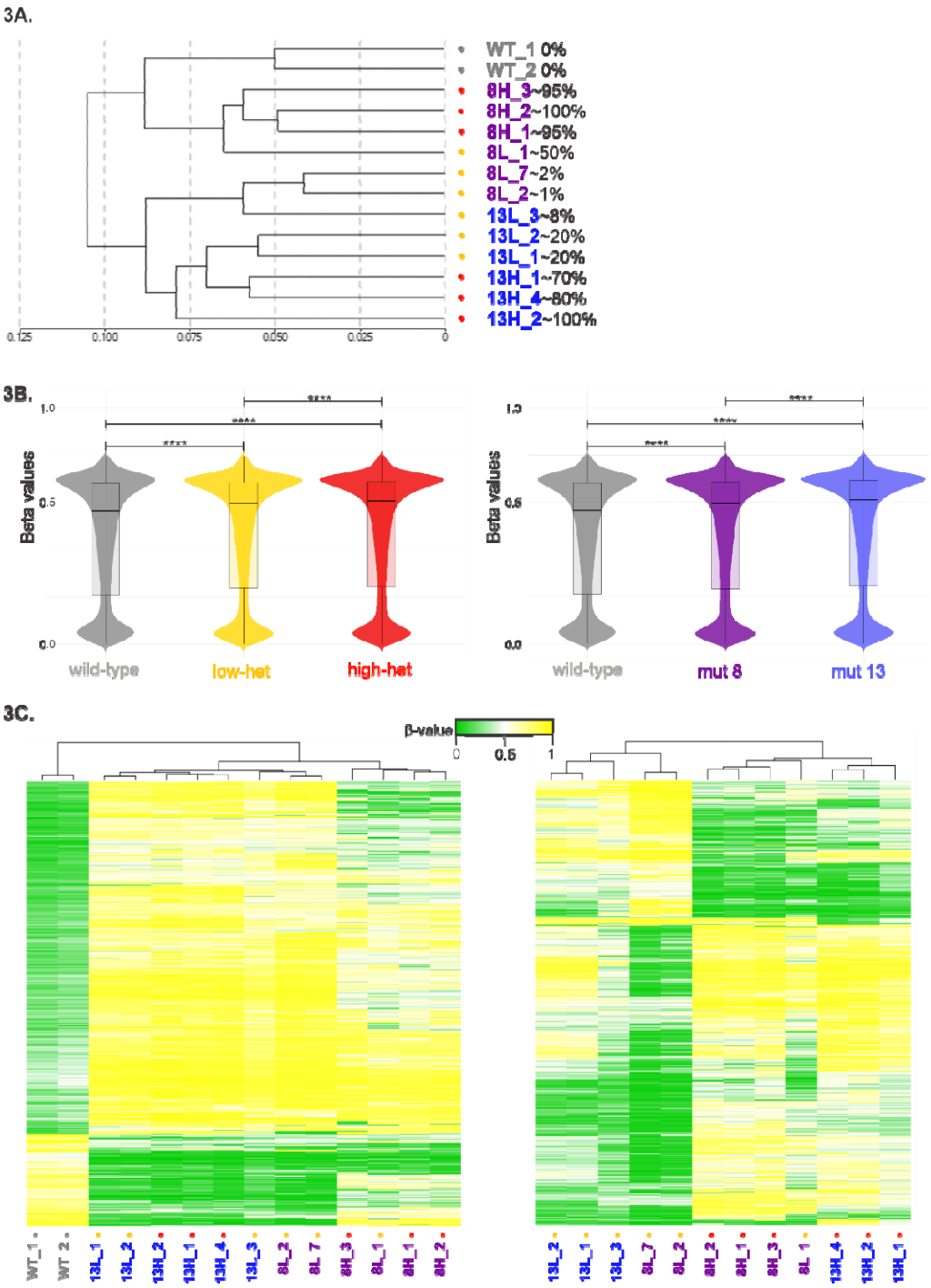

Figure 3. **Genome wide methylation pattern differs between groups. Analysis of over 850,000 CpG sites using Illumina´s Infinium EPIC 850k. 3A**. Full methylation pattern sample dendrogram obtained through Illumina´s GenomeStudio Software®. Unsupervised hierarchical cluster using Manhattan's distance and average linkage clustering method. Next to each sample name, the approximate heteroplasmy percentage is shown. The samples cluster according to mutation type (or wild-type) and heteroplasmy. **3B.** Violin plots and Box plot graphs generated from average beta values of each subgroup. Left panel comparison according to heteroplasmy subgroups. Right panel comparison between mutation types. ****p<0.0001 Wilcoxon matched-pairs signed rank test for paired comparisons of mean values at each CpG site. **3C**. Heat-map

showing Unsupervised hierarchical clustering (Manhattan's distance + average linkage) of the top significantly ($p<0.05$) differentially methylated regions (DMRs). Δ mut-wt > 0.4 or <-0.4 (left panel) and Δ high-low > 0.27 or <-0.27. Column cluster dendrogram is shown, row clustering was performed but dendogram is hidden. Throughout figure 3, samples are highlighted with different colors according to mutation type (grey= wild-type, blue= m.13513G>A, purple= m.8344A>G) and heteroplasmy (grey= 0%, gold= low-heteroplasmy, red= high-heteroplasmy).

The nDNA methylation profile contributes to explaining the distinct fate behaviors of high and low heteroplasmy cells.

Given the differences observed in the global nDNA methylation analyses above, we aimed to examine the behavior of these cybrids in the presence or absence of DNA methylation modulators.

Intriguingly, high-mutant cybrids showed a higher proliferation rate than their low-heteroplasmy counterparts, a phenomenon which was abolished when DNA methylation was perturbed (Fig 4A, Fig. S3). Furthermore, high heteroplasmy cells were more sensitive to apoptosis upon treatment with 5-azacytidine or decitabine (Fig 4B). To reinforce the importance of DNA methylation for this observation, we also checked the apoptosis level of the m.13513G>A DNMT1 knock-downs and saw similar effects. The 13L mutants did not increase their apoptotic rate in the presence of demethylating agents nor DNMT1 knockdown. The 8H mutants showed overall an increased apoptosis level compared to the 13H mutants.

These data suggest that high-heteroplasmy cells *depend on* their nDNA methylation marks to proliferate and avoid apoptosis.

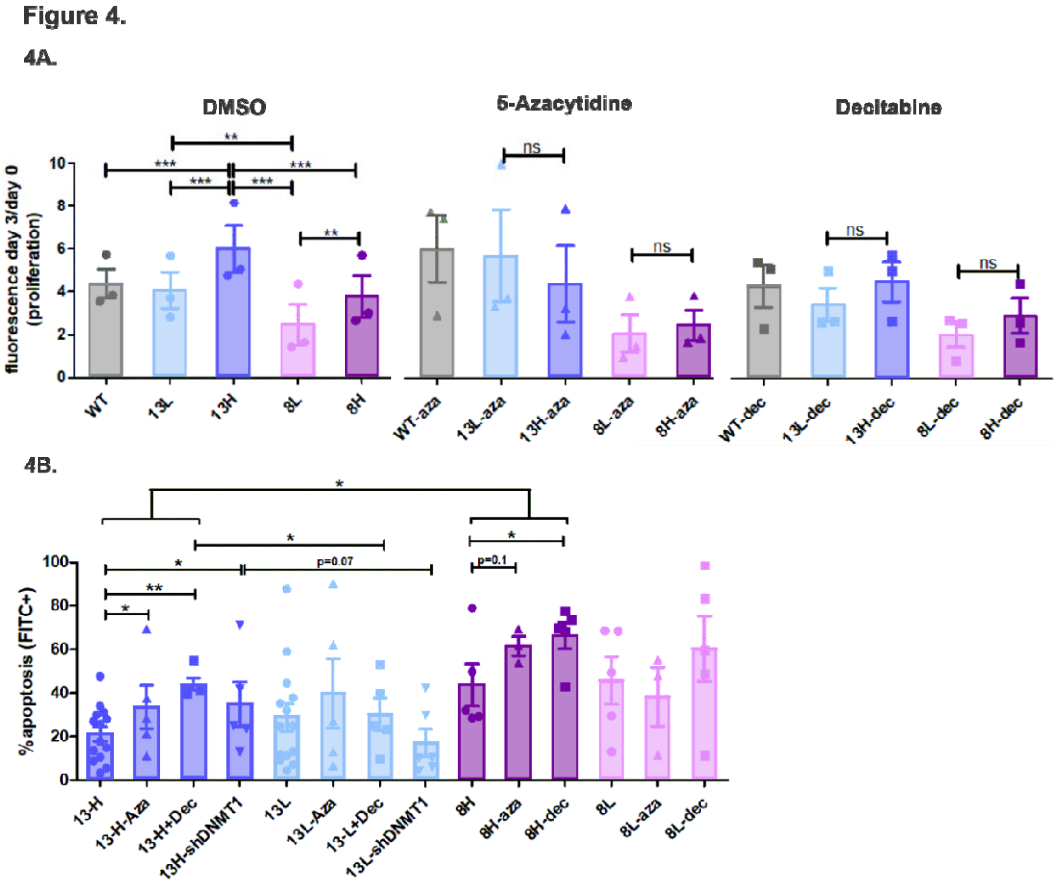

Figure 4. **The nDNA methylation profile determines differential proliferation and apoptosis of cybrids. 4A**. Differential proliferation of cells treated with vehicle (DMSO, left panel), 5-azacytidine (aza) 1µM-3 days (middle panel), decitabine(dec) 1µM-3 days (right panel). Other drug concentrations with similar effects are shown in Fig S3. **p<0.01. ***p<0.001. Repeated Measures ANOVA, Newman-Keuls Multiple Comparison Test. N=3 experiments. **4B**. Apoptosis assay with Annexin V-FITC, Flow cytometry. Using a threshold based on autofluorescence in the Annexin V-FITC histogram, cells were designated as apoptosis (+) or (−) for quantification. *p<0.05, **p<0.01, one-tailed, unpaired Student´s t-tests. N ≥3 independent experiments.

To understand the DNA methylation marks that could be contributing to this phenotype, we went back to our EPIC 850k beta values and compared the high versus low heteroplasmy´s epigenetic signature (for both ´13´ and ´8´ mutants). We found that CpG sites with differential methylation were associated to genes with an enriched participation in 'survival' pathways (Fig 5A, Supplementary file 1). Genes in these pathways were mostly hypermethylated as had happened across the genome. As a representative of this functional group, ESR1 has been described as a tumor suppressor gene in various cancers, including osteosarcomas[59,60]. In these cancers, ESR1´s promoter is hypermethylated and therefore underexpressed[61,62]. Additionally, its expression is enhanced by decitabine treatment, leading to a reduction in both proliferation and metastasis[61]. Since the cybrids we worked with have an osteosarcoma nuclear background (143B), and ESR1 was in the list of hypermethylated genes in high-heteroplasmy cells (Fig 5A) we looked in detail at the differential methylation of the ESR1 locus (Fig 5B) and compared the ESR1 expression, namely the estrogen receptor 1 protein between the 13H and 13L lines (Fig 5C). We found hypermethylation of the whole ESR1 locus (Fig 5B), a trend to lower expression in high heteroplasmy

cells and a significant increase after treatment with decitabine (Fig 5C). Such treatment appeared to have no or the opposite effect in the 13L line. Thus, the variation in the abundance of ESR1 (among other differentially methylated genes) could be contributing to the distinctive growth and survival behavior of heteroplasmic cells.

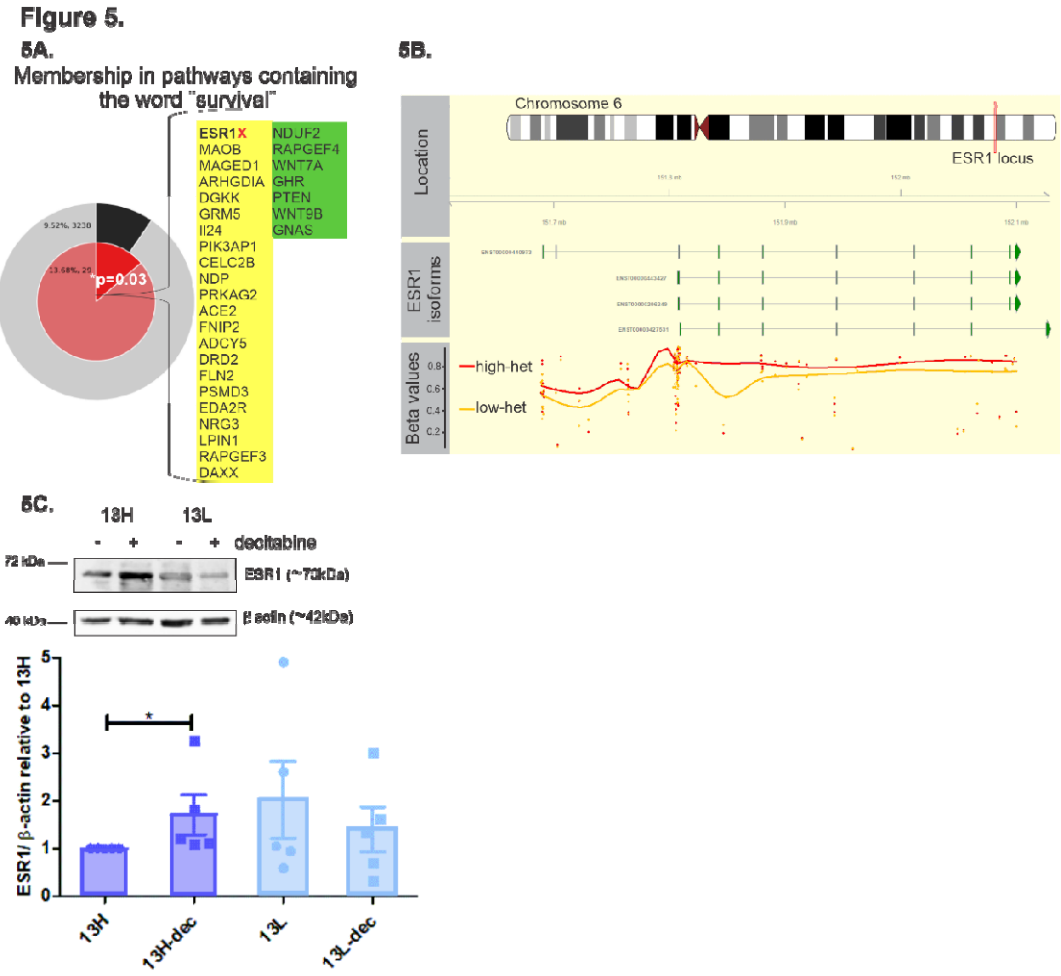

Figure 5. Genes related to survival are differentially methylated in high versus low heteroplasmy cybrids. 5A. Metascape analysis of the differentially methylated genes that resulted from 850k EPIC (222 genes meeting differentially methylated criteria -see methods section- of which 168 =75.7% were hypermethylated), Supplementary file 1. The Metascape pie chart compares membership in 'survival pathway' of our gene list (inner pie) and the proportion of survival genes that would appear by chance in coding regions (outer pie). The significantly low p-value confirms that 'survival' is overrepresented in our gene list, emphasizing its relevance to our hypothesis. The genes that determine the enrichment in survival pathways are listed next to the pie, in yellow are the hypermethylated and in green the hypomethylated genes for the high-heteroplasmy versus low-heteroplasmy group. In Supplementary file 1, these genes are displayed next to the pathways to which they belong. Marked with a red cross is the ESR1 gene which is analyzed further in 5B and 5C. **5B.** Differential DNA methylation of the ESR1 locus. The top panel represents the chromosomal location of ESR1. The middle panel depicts ESR1 transcript isoforms (ENSEMBL IDs), with exons as green boxes and introns as connecting lines. The bottom panel displays DNA methylation data from the Illumina Infinium MethylationEPIC array (850K) for the ESR1 locus. Beta values, which range from 0 (unmethylated) to 1 (fully methylated), for CpG probes in the region. Average beta values for each group (high and low heteroplasmy) of the individual CpG sites are shown as dots. The red and gold lines are

LOESS (locally estimated scatterplot smoothing) curves, that provide a smoothed representation of methylation differences across the region, confirming a higher methylation level for the high heteroplasmy samples. **5C**. Representative western blot and quantification of ESR1 protein in the m.13513G>A cybrids (13H= high-heteroplasmy, 13L= low-heteroplasmy) with and without 3-day 1µM decitabine (dec) treatment. *p<0.05, Wilcoxon matched-pairs signed rank test. N= 5 independent experiments.

DNA methylation modulators influence cybrid cells´ mitochondrial function.

Because these cybrid cells have an altered metabolic state to begin with, we studied whether it was influenced further by DNA methylation modulators. We analyzed the oxygen consumption rate of cells treated with decitabine. We tested 13H (Fig 6), wild-type cybrids and mutated mouse embryonic fibroblasts (m.5024C>T) with intermediate heteroplasmy (~50%) (Fig S4). All cells tested increased their oxygen consumption when treated with decitabine. This was not accompanied by increased levels of oxidative phosphorylation complex proteins (Fig S5).

Considering that high-heteroplasmy cells have worse mitochondrial function and that their growth and survival is impaired with decitabine treatment, we reasoned that oxygen may be mishandled by the most dysfunctional cells. Therefore, we investigated the levels of reactive oxygen species (ROS) of the different cybrids before and after treatments. Indeed, decitabine increased the level of ROS for the 13H and 13L cybrids and showed a tendency to do the same in the 8H and 8L cells (Fig 6C). Knock down of DNMT1 was not enough to mimic decitabine´s action (data not shown). Hence, even though oxygen consumption increased with DNA methylation inhibition, decitabine treatment led to an increase in ROS, more pronounced in the high-heteroplasmy cells, probably contributing to their enhanced susceptibility to apoptosis with the drug.

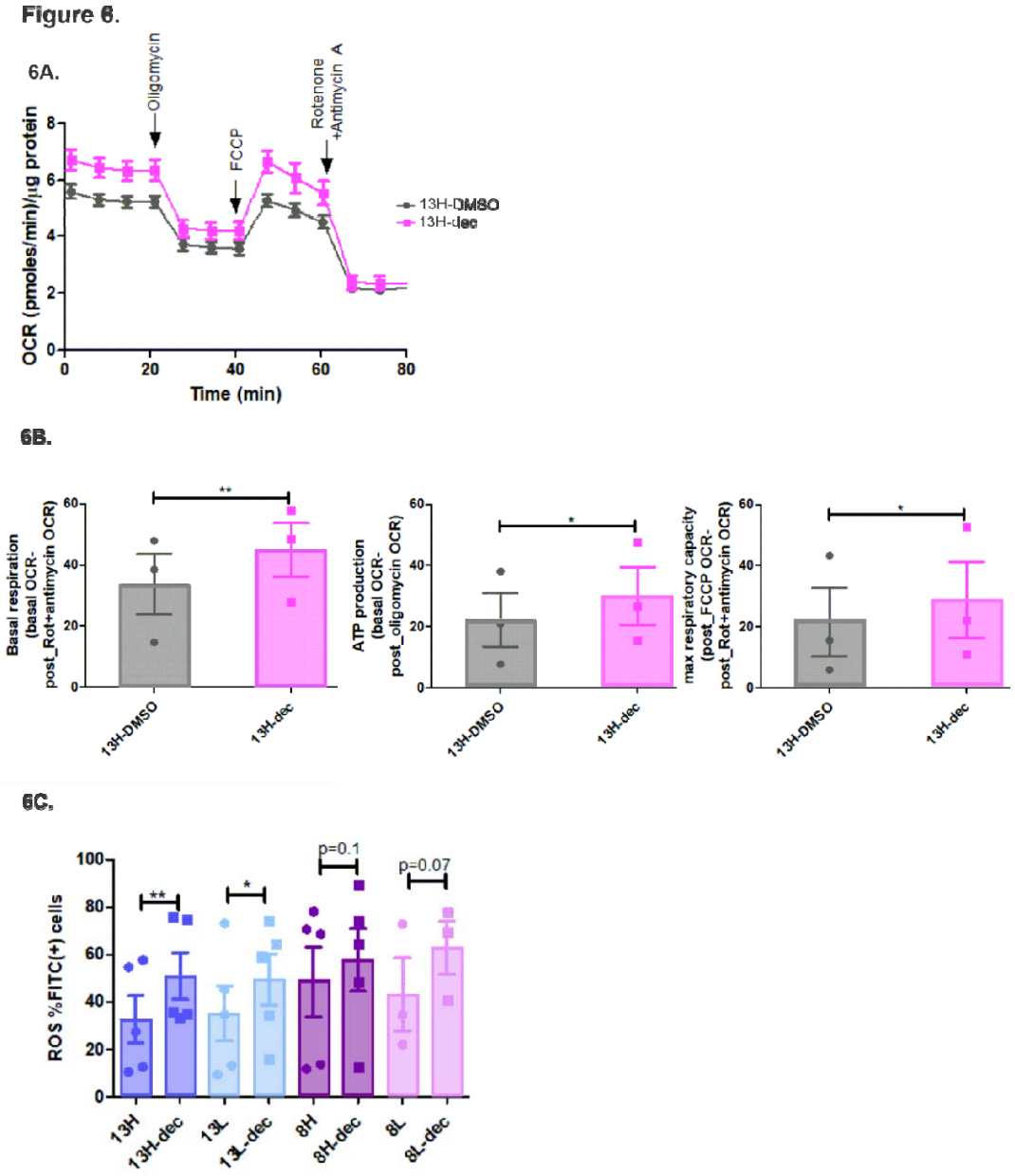

Figure 6. **DNA methylation inhibitor decitabine impacts mitochondrial function. 6A and 6B**. High-throughput oxygen flux analysis using Seahorse®. 13H cells were submitted to a mito-stress test. **6A.** Oxygen consumption rate (OCR) kinetics with sequential addition of Oligomycin, FCCP, Rotenone+ Antimycin A. **6B.** Quantification of key mitochondrial function parameters. Left panel: Basal respiration (OCR at baseline- OCR post_Rot+Antimycin). Middle panel: ATP production (OCR Basal respiration – OCR post_oligomycin). Right panel: Maximal respiration capacity (OCR post_FCCP – OCR post_Rot+Antimycin). All parameters increased in the decitabine (dec) conditions 1µM 1-day treatment. **p<0.01, *p<0.05. Two-tailed, paired Student´s t-test. N=3 independent experiments. **6C.** Evaluation of reactive oxygen species (ROS) through flow cytometry using DCF-DA (FITC): % of FITC(+) cells were determined using an autofluorescence based threshold. % of cells testing positive for ROS were compared using one-tailed, paired Student´s t-test. **p<0.01, *p<0.05. N= 3-5 independent experiments, Decitabine (dec) 1µM 3-day treatment versus controls treated with DMSO.

DNA methylation inhibitors lower mtDNA heteroplasmy in cultured cells

Given the notable nDNA methylation difference between cells with varying heteroplasmies and the divergent behavior upon treatment with DNA methylation modulators, we ventured to see if heteroplasmy could be modified when cells were treated with these methylation erasers. Given that the most pronounced differences were in the ´13´ cybrids we chose that line for the following experiments. Mutant mtDNA ratios diminished ~15% consistently in 13H cybrids treated with decitabine (Fig 7A). Mitophagy was not enhanced by the drugs (Fig S6A), nor did mtDNA content vary significantly (Fig S6B).

In tissues from patients with mitochondrial diseases high and low heteroplasmy cells can coexist[46,63]. So, taking into account our previous results, in which high heteroplasmy cybrids selectively died and lost their proliferative advantage upon treatment with demethylating agents, we hypothesized that there could be a *selection* towards the low-heteroplasmy cells when treated with these drugs. Maybe the 13H cybrids were not as pure of a clone and had a proportion of 13Ls which made their heteroplasmy sensitive to DNA methylation modulation.

To test this, we deliberately mixed 13H and 13L cybrids before treating them with DNA methylation inhibitors. Additionally, we labelled the 13L cells with a green dye in order to trace the percentage of them upon DNA methylation inhibition. When the mixture of cells was treated with the drugs, the percentage of green cells increased (Fig 7B and 7C) and accordingly, the heteroplasmy of the mixture decreased (Fig 7D).

Figure 7.

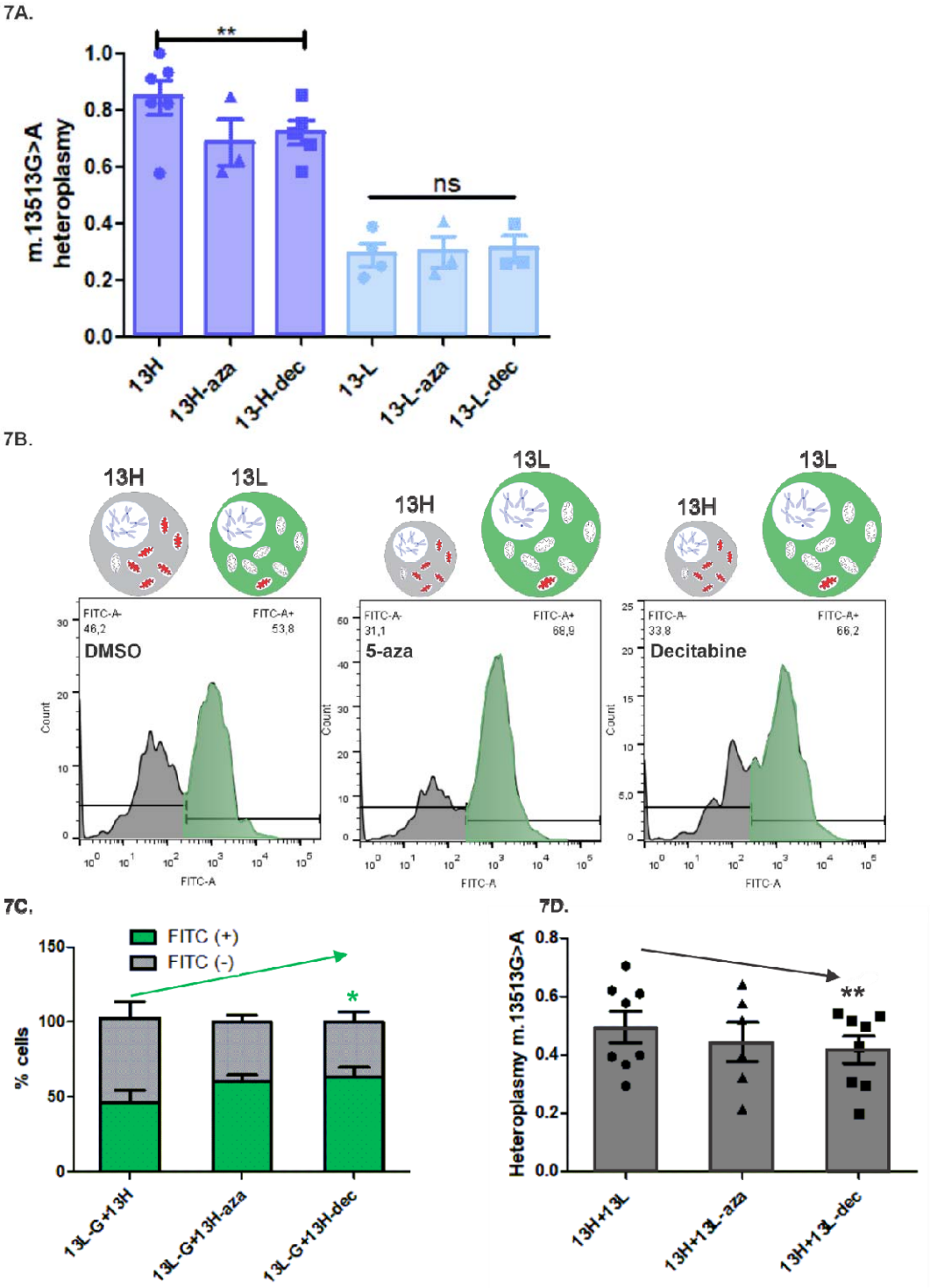

Figure 7. **Treatment with DNA methylation modulators lower m.13513G>A cybrids´ heteroplasmy. 7A.** m.13513G>A heteroplasmy was measured using SYBR green based RT-qPCR. M.13513G>A high heteroplasmy cells (13H) decreased their heteroplasmy when treated with decitabine (dec) 1µM- 3days. **p<0.01. One-tailed, paired Student´s t-test. N= 5 independent experiments, treatment with 5-azacytidine (aza) showed the same tendency (N=3, p=0.1). **7B.** Low-heteroplasmy m.13513G>A cybrids traced with green cell tracker (13L-G) were

mixed in equal proportions with undyed high-heteroplasmy cybrids (13H) before treating them with DMSO, 5-azacytidine(aza) or decitabine(dec). After 3-day treatment they were collected and the percentage of green cells= %FITC(+)= (13L-G) was measured through flow-cytometry. **7C.** Quantification of the percentage of FITC (+) = 13L-G and FITC (-) =13H cells after treating them with DMSO, azacytidine or decitabine. *p<0.05 One-tailed, paired Student´s t-test. N= 4 independent experiments. **7D**. m.13513G>A heteroplasmy of the mixture of 13H+13L cells treated with DMSO, 5-azacytidine or decitabine was measured using SYBR green based RT-qPCR. **p<0.01 One-tailed, paired Student´s t-test. N= 6-8 independent experiments. Treatment with 5-azacytidine showed the same tendency (p=0.07).

The DNA methylation inhibitor decitabine reduces mtDNA heteroplasmy in an *in vivo* xenograft model by erasing nuclear DNA methylation marks.

After appreciating the effects of DNA methylation inhibitors on the particular heteroplasmy cybrids regarding cell fate and mutation load, we aimed to scale these observations to a more physiological *in vivo* model. For this, we implanted subcutaneously 13H, 13L and a mixture of 13H and 13L cybrids in NSG mice. After tumors were palpable (~2 weeks after injection), we treated half the mice with decitabine and the other half with its vehicle (DMSO) for 8 days and monitored tumor growth. Post-mortem analysis of the tumors included nuclear and mitochondrial DNA methylation pattern assessment (to ensure dectiabine´s in vivo action) and m.13513G>A heteroplasmy (to test its potential therapeutic facet) (Fig 8A). We found even more striking effects to what we had observed in cell culture. As expected, and as reported before[62,64,65] overall tumor growth was decelerated in the decitabine group (Fig S7A, left panel). When dissecting the different tumor types, the growth of high-heteroplasmy and ¨mixed¨ tumors was significantly attenuated with decitabine treatment, whereas the low-heteroplasmy ones did not respond to the demethylating agent (Fig 8B). When comparing the growth rate of the purely high or low mutant tumors within the controls (vehicle-DMSO) and in the treated mice (decitabine) there were no significant differences. Although, in the untreated group, the high-mutants tended to grow faster than the low-mutants whereas the opposite was true for the treated group (Fig S7A, right panel), in line with what we had seen in cell culture. In conclusion, there is a distinctive tumor growth and sensitivity to DNA methylation modulation in relation to heteroplasmy that we thought could be exploited to shift heteroplasmy. Additional information regarding final tumor sizes is available in Fig S7B and its legend.

Regarding the drug´s impact on the tumors´epigenome, as expected, decitabine reduced overall DNA methylation, and DNA methylation comparisons of high versus low heteroplasmy tumors mirrored cultured cells´ EPIC results (Fig 8C, left panel). The method we used to assess methyl-CpGs in this occasion (MinIOn Nanopore technology®) is especially useful for short genomes such as the mtDNA, so to the contrary of EPIC, mtDNA data was overrepresented, and we confirmed the same observations reported with EPIC. As reported before[66,67], mtDNA methylation was minimal compared to the nuclear one and importantly, decitabine had *no* significant effect on this pattern (Fig 8C, right panel, Fig S7C). Mean methylation levels across the mitochondrial chromosome even showed an opposite trend (higher methylation for the treated tumors) (Fig 8C, Fig S7C). Therefore, we can confirm that the high-low heteroplasmy differential behavior is determined through nuclear changes and that decitabine´s effect is centered in nuclear epigenetic modification.

Finally, and most importantly, we checked the impact of decitabine on heteroplasmy of all tumors. Again, as we had seen in the cell culture experiments, decitabine reduced the mutation load significantly in the high-heteroplasmic tumors and the mixed heteroplasmy ones. Heteroplasmy from the low group was not modified by the demethylating drug (Fig 8D, Fig S7D). Notably, the heteroplasmy reduction in the *in vivo* model was more pronounced than in cell culture, achieving a 22% reduction (7% more than in cells) for the high-heteroplasmy tumors and a 40% reduction, (doubling the effect in cells) for the mixed heteroplasmy ones.

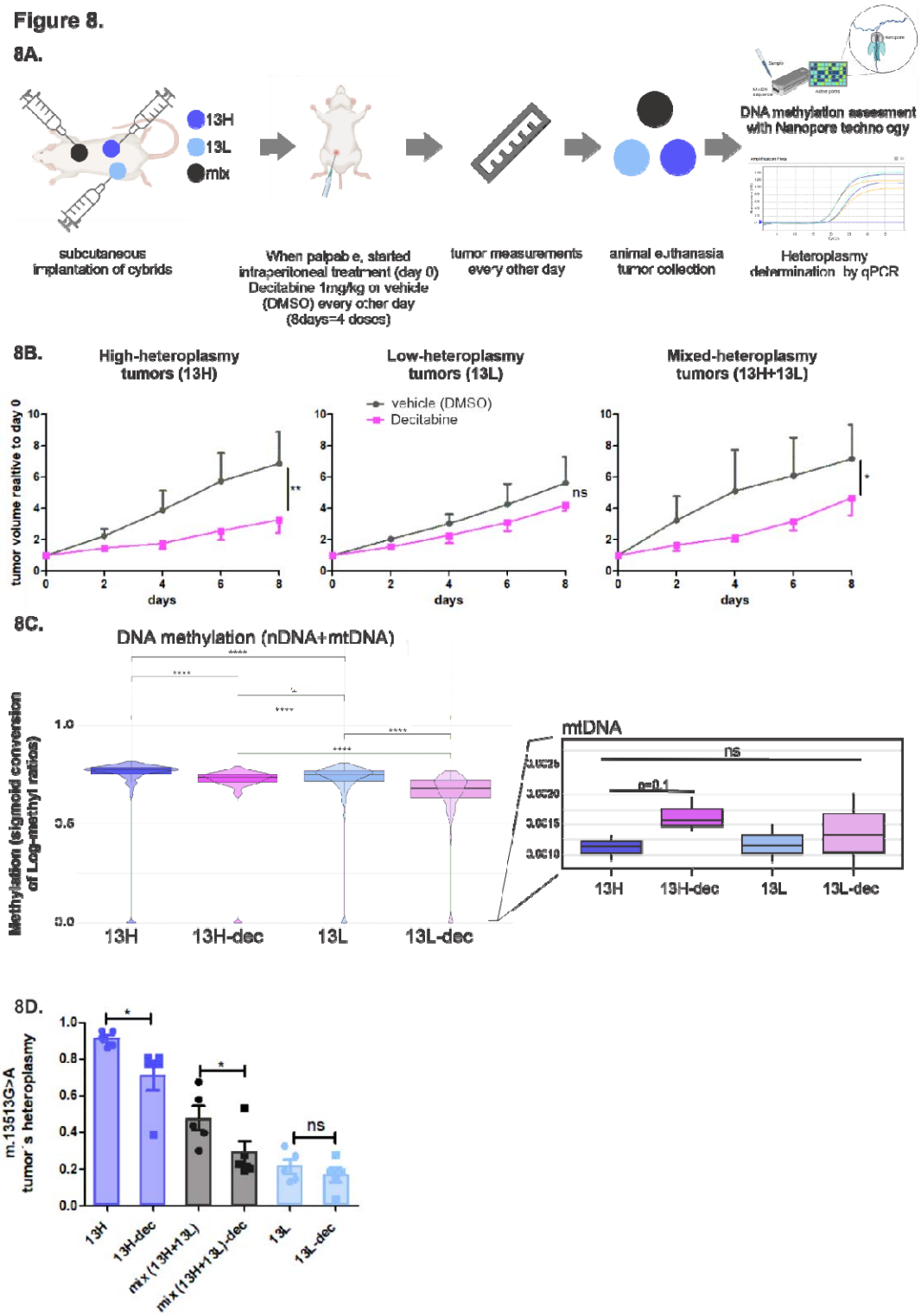

Figure 8. Decitabine impacts tumor growth and m.13513G>A heteroplasmy in a xenograft model. 8A. Xenograft experiments sketch. **8B.** Tumor growth in the different tumor types and treatments. Decitabine decelerates the growth of the high and mixed heteroplasmy tumors. Tumors were measured every other day, and their growth was quantified relating to tumor volume at day 0. **p<0.01, *p<0.05, Two-way ANOVA test. N= 10 mice (5 for decitabine group, 5 for control group). ns= not statistically significant. **8C.** Tumor DNA methylation assessment

through Nanopore sequencing. To transform the log-methyl ratio (LMR) into a probability-like measure of methylation, we applied the logistic (sigmoid) function: $P=1/(1+e^{-LMR})$. This transformation maps LMR values to a range between 0 and 1. Left panel shows values across all chromosomes (including mtDNA). All conditions show significant differences exhibiting, as in EPIC results, higher methylation in the 13H tumors and confirming decitabine´s demethylating effect. Right panel highlights mtDNA´s extremely low methylation values with no significant differences between conditions and *no* demethylating effect of decitabine, even showing a tendency of higher methylation in the treated tumors, ****p<0.0001, *p<0.05, Wilcoxon matched-pairs signed rank test of paired comparisons of the median methylation values for each chromosome. N= 3 tumors from each condition 13H, 13h-dec, 13L, 13L-dec. **8D.** m.13513G>A heteroplasmy of the different tumors with and without decitabine treatment. Heteroplasmy was assessed using SYBR green based RT-qPCR. *p<0.05 One-tailed, unpaired Student´s t-test. N= 5 tumors for each group.

DISCUSSION

Our study provides new insights into how mitochondrial health influences nuclear epigenetics[22,23,68], and how nuclear DNA methylation in turn, impacts mitochondrial function.

Specifically, we show that both the *type* (mtDNA mutation) and *intensity* (heteroplasmy) of mitochondrial dysfunction distinctly shape nuclear epigenetics. In line with our previous findings, we confirmed that severe mitochondrial impairment correlates with increased nDNA methylation [23]. This epigenetic patterning is especially important for the survival of high-heteroplasmy cells supporting their proliferation and helping them avoid apoptosis. This aligns with previous findings in 143B osteosarcoma cells, which share the nuclear background of our cybrid model, showing that impaired respiration can paradoxically protect cells from apoptosis [69]. Consistently, disrupting nuclear methylation selectively compromised high-heteroplasmy cells, as demonstrated by our cell culture and xenograft model, where decitabine treatment altered nuclear but not mitochondrial DNA methylation. While mtDNA methylation remains debated[57,67], we observed only minor levels in our cell lines with no significant differences across comparisons, reinforcing that major epigenetic shifts triggered by mitochondrial dysfunction occur in nuclear DNA. These findings emphasize the pivotal role of mitochondria-to-nucleus communication for the epigenetic adaptation in a mitochondrial dysfunctional scenario.

After confirming that mitochondrial function molds the nuclear epigenome, we demonstrated that, conversely, nDNA methylation modulation has an impact on mitochondrial function, and most interestingly on mtDNA heteroplasmy. Our studies showed that FDA approved DNA methylation inhibitors, particularly decitabine, had an impact on mitochondrial respiration, reactive oxygen species production, proliferation and apoptosis distinctively according to the level of heteroplasmy.

Building on these insights, we visioned that the selective vulnerability of high-mutant heteroplasmic cells towards DNA methylation inhibitors could be a tool to lower heteroplasmy and proved their capability to do so. By targeting these methylation patterns with drugs like decitabine and 5-azacytidine, the growth and survival of high heteroplasmy cells was impaired, resulting in the enrichment of low-heteroplasmy cybrids, decreasing the overall mutant load. This was shown both in cell culture and most pronouncedly in an *in vivo* xenograft model.

This study introduces a groundbreaking approach to addressing mitochondrial heteroplasmy by modulating nuclear epigenetics rather than directly targeting mtDNA.

This proof of concept opens a new window for epigenetic modifiers in the treatment of mitochondrial disorders. Unlike other methods that require delivery of foreign molecules to the mitochondria[11,13–15,27,70], our strategy exploits endogenous nuclear-mitochondrial communication pathways. Furthermore, this approach avoids transient mtDNA depletion—a common challenge with nuclease-based therapies [15,16,27] —and relies on shifting the cellular population dynamics to favor healthier mitochondrial compositions. The use of clinically approved drugs may also facilitate the translation of this strategy into clinical practice.

While promising, our findings come with limitations. The use of cybrid cell lines and xenograft models, though powerful, may not fully capture the complexity of tissues most affected by mitochondrial diseases, particularly post-mitotic ones with minimal cell turnover. On the one hand, DNA methylation inhibitors require proliferating cells to exert their effect[71–74]. On the other hand, the selective elimination of high-heteroplasmy cells may have functional consequences that warrant further exploration. The increasing availability of mtDNA disease animal models[75–78] certainly compels additional *in vivo* research to test the possibility to lower heteroplasmy and alleviate symptoms with epigenetic drugs in these settings.

Investigating combination therapies—such as pairing DNA methylation inhibitors with mitochondrial-targeted antioxidants[79,80], or post-mitotic tissue regenerating strategies[81–84]—could further enhance therapeutic outcomes by increasing the drugs´ action and mitigating potential side effects.

Moreover, beyond mitochondrial diseases, the susceptibility of cells with very poor mitochondrial function to epigenetic modulation holds potential for applications in oncology. Although DNA methylation modulators are already used in this field[24,25], these drugs could be specifically efficient in cancers with particularly unfit mitochondria[85], broadening the clinical utility of the findings of our work.

In conclusion, our study identifies a DNA methylation-dependent adaptive survival mechanism in high-heteroplasmy cells, which can be selectively targeted to reduce mtDNA heteroplasmy. This work introduces epigenetic modulation as a novel strategy to shift mitochondrial mutant load, offering a promising therapeutic avenue for mitochondrial diseases and potentially other conditions involving mitochondrial dysfunction.

AUTHOR CONTRIBUTIONS: LM conducted the research project, planned the experiments and provided main funding. MJP, RBC, SMR and LM performed the experiments. SRL , MTB processed big data and performed statistical analysis. CTM collaborated with cell lines, reagents, equipment and experimental guidance. LM wrote the paper with the help of CTM. All authors read and approved the final manuscript.

DATA AVAILABILITY STATEMENT: All data supporting the findings of this study are available in the main text and supplementary materials and GitHub repository. Any additional information can become available upon request.

FUNDING:

2021 UMDF Accelerator prize: Modulation of the nuclear epigenome as a new strategy for mtDNA heteroplasmy shift. Lía Mayorga.

Wood-Whelan research fellowship 2019 for a short stay at Moraes Lab (Miller School of Medicine, University of Miami, USA). “Modulation of the epigenome as a new strategy for mtDNA heteroplasmy shift”

PICT 2019-00449 (PICT joven 2019): Shift de la heteroplasmia mitocondrial por modulación del epigenoma nuclear: posible tratamiento para enfermedades mitocondriales.

Programa de Redes Federales de Alto Impacto, proyecto de investigación: Genómica Clínica de Enfermedades Poco frecuentes. Ministerio de Ciencia, Tecnología e Innovación de la Nación Argentina. 2023.

The work in the Moraes Lab is funded by the National Institutes of Health (NIH) award R01EY010804, the Army Research Office (W911NF-21-1-0248), the Muscular Dystrophy Association (MDA 964119), The Research to Prevent Blindness Stein award and the Florida Biomedical Foundation (21K05).

ACKNOWLEDGEMENTS

Firstly, we thank the United Mitochondrial Disease Foundation, especially the families that voted for this project, and of course, the donors that contributed with the funding for the accelerator prize. This prize made the project possible. We thank the rest of the funding that also contributed to this work. We also thank Dr. LS. Mayorga (manuscript revision—IHEM, Mendoza, Argentina) and Dr M. Roqué (manuscript revision—IHEM, Mendoza, Argentina).

DECLARATION OF COMPETING INTEREST

The authors declare no conflicting interest.

Supplementary figures

Figure S1.

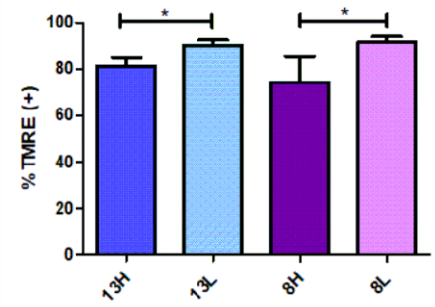

Fig S1: Differences in mitochondrial membrane potential between high and low heteroplasmy cybrids. measured with TMRE through Flow cytometry. Using a threshold based on autofluorescence in the TMRE-PE histogram, cells were designated as TMRE (+) or (−) for quantification. One-tailed unpaired Student´s t-tests. N >6 independent experiments. *p<0.05.

Figure S2.

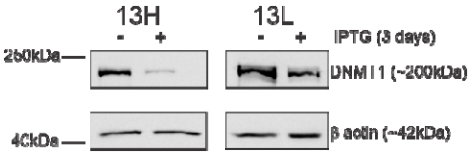

Fig S2: DNMT1 knockdown control in ´13´ cybrids. DNMT1 expression through Western Blot in the stable cell line of m.13513G>A low (13L) and high-heteroplasmy (13H) cybrids with the mammalian pLV[shRNA]-LacI: T2A:Puro-U6/2xLacO>hDNMT1[shRNA#1]. 3-day treatment with IPTG: isopropyl-galactosidase(TRANS®) 500 µM was installed to decrease DNMT1 expression.

Figure S3.

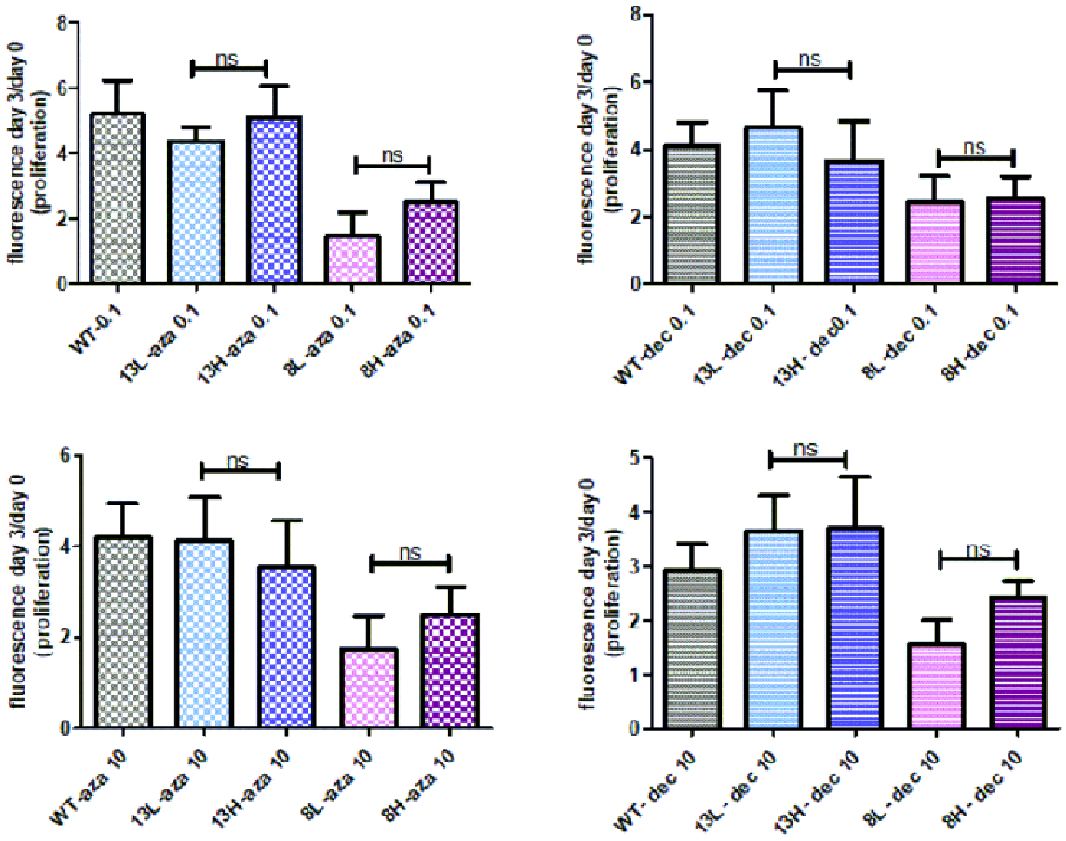

Fig S3: DNA methylation inhibitors reduce differences in proliferation rates of high-low heteroplasmy cybrids. Differential proliferation of cells treated with 5-azacytidine (aza) and decitabine (dec) 0.1µM (upper panels) or 10 µM (lower panels) for 3 days. Repeated Measures ANOVA, Newman-Keuls Multiple Comparison Test. Comparisons between high and low heteroplasmies are stood out to compare with Fig 4A. ns= not significant. N=3 experiments.

Figure S4

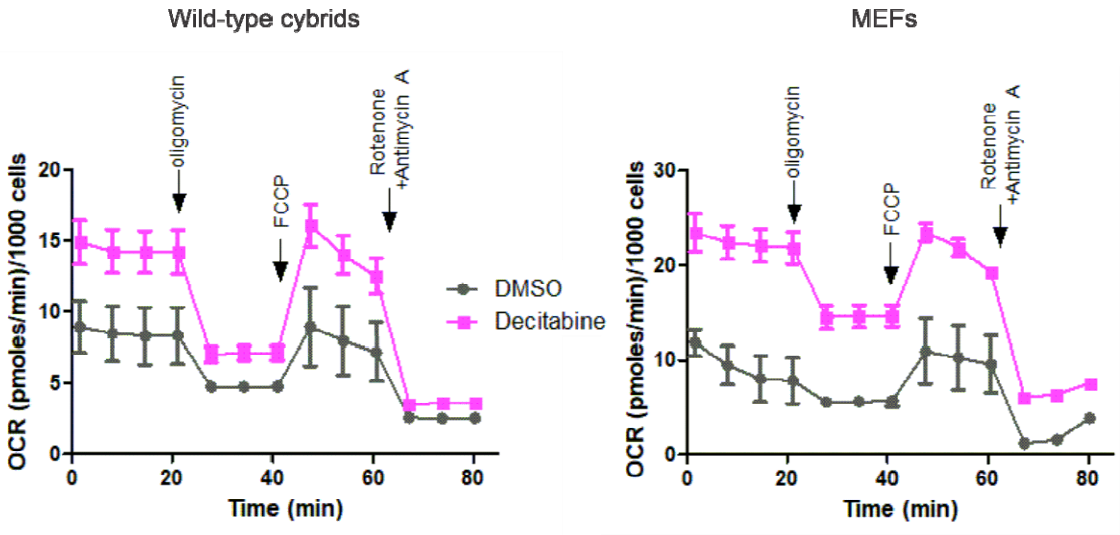

Fig S4: Decitabine increases oxygen consumption rate in different cell lines. High-throughput oxygen flux analysis using Seahorse®. wild-type cybrids and m.5024C>T MEFs were submitted to a mito-stress test. Oligomycin, FCCP, Rotenone+ Antimycin A were added sequentially. Basal respiration (OCR at baseline- OCR post_Rot+Antimycin). ATP production (OCR Basal respiration – OCR post_oligomycin). Maximal respiration capacity (OCR post_FCCP – OCR post_Rot+Antimycin) all increased in the Decitabine (dec) conditions 1µM 1-day treatment.

Figure S5.

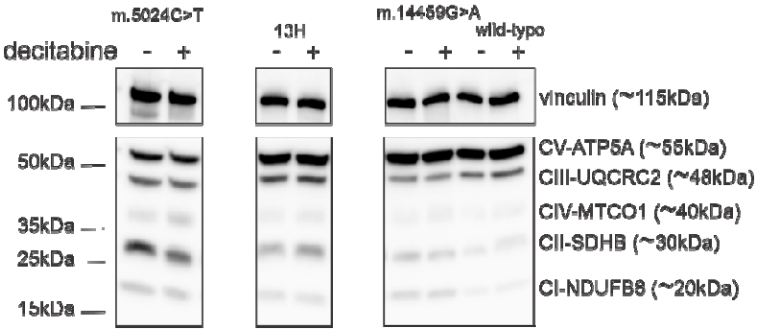

Fig S5: DNA methylation inhibitor decitabine does not change significantly the expression of mitochondrial complexes. Western blot to study the expression of mitochondrial complexes in different cells with and without decitabine treatment 1-day 1µM. m.5024C>T ~50% heteroplasmy MEFs, 13H= m.13513G>A high-heteroplasmy~80% cybrids, m.14459G>A fibroblasts~95% heteroplasmy.

Figure S6.

S6A.

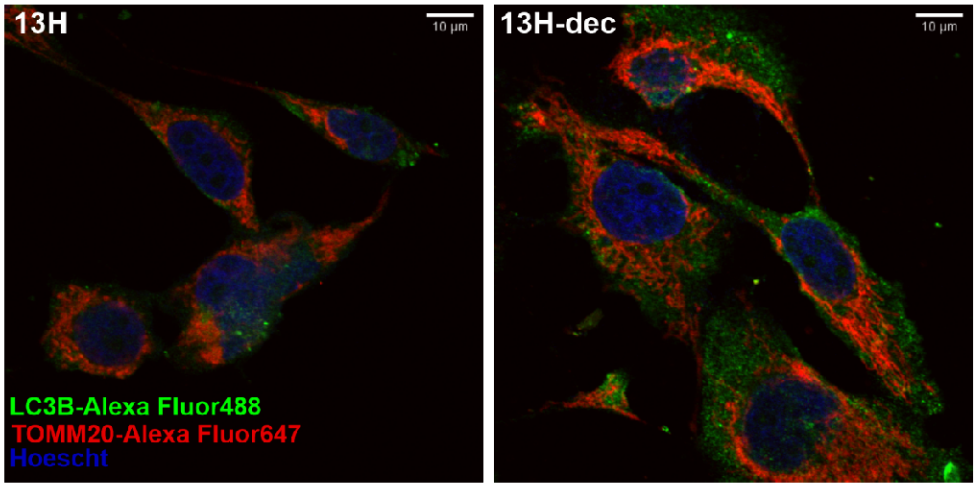

S6B.

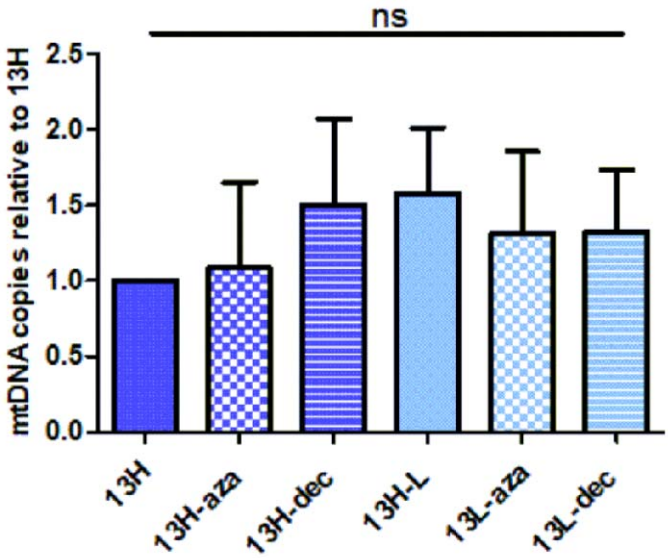

Fig S6: DNA methylation modulators do not impact mitophagy nor mtDNA content. S6A. Confocal Immunofluorescence Microscopy. Confocal laser micrographs depict indirect immunofluorescence staining of LC3B (labeled with AlexaFluor 488 in green) and TOMM20 (labeled with AlexaFluor 647 in red) within m.13513 high heteroplasmy cybrids (13H) treated with decitabine 1µM-3days (right panel) or DMSO (left panel). The cells´ nuclei were stained with Hoescht (blue). Colocalization of the two proteins is not evidenced. **S6B.** mtDNA content. mtDNA content was measured with SYBR green based RT-qPCR relativizing the m.13513 ´all´ amplicon to the nuclear gene B2M, quantified using ΔCT method= $2^{-(allCT-B2MCT)}$. One-way ANOVA, Tukey´s multiple comparison test.

Figure S7.

S7A.

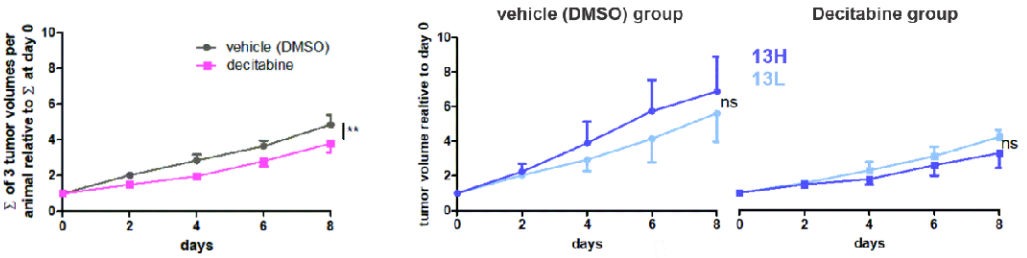

S7B.

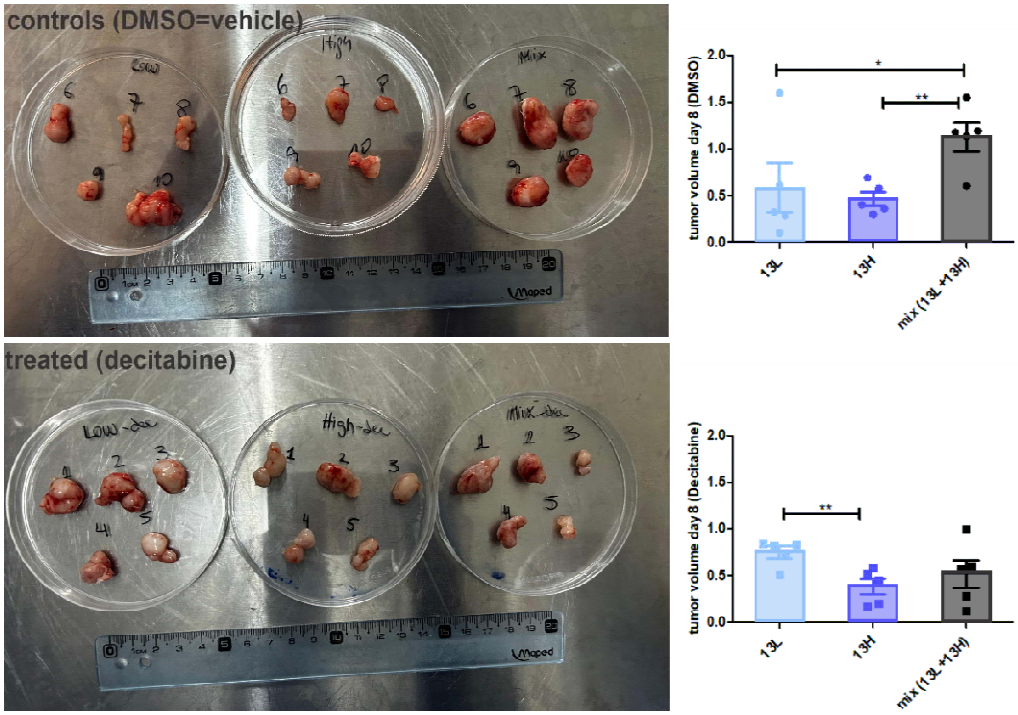

S7C.

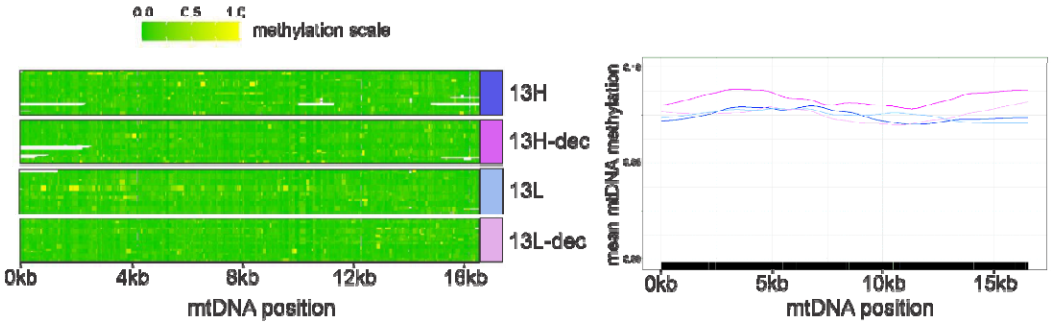

S7D.

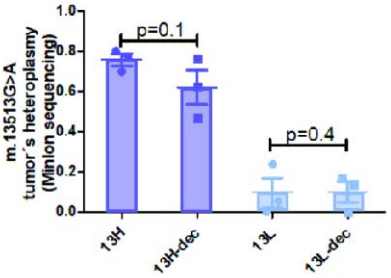

Fig S7: Further characterization of xenograft experiments regarding tumor growth, tumor volume, mtDNA methylation and heteroplasmy. S7A. Left panel: overall tumor growth in mice in the control (DMSO) and treated (Decitabine) group. The volumes of the 3 tumors per animal were added up every measurement day and that sum was relativized to the sum of tumor volume of day 0 per animal. **p<0.01, Two-way ANOVA test. Right panel: comparison of the high and low heteroplasmy tumor growth within the control and treated group. **S7B.** Final tumor size assessment at day 8. It is worth clarifying that tumor sizes started out uneven in order to have all 10 mice under treatment at the same time. Therefore, final tumor volumes *do not* represent their growth rate. Anyhow, we can stand out that the mixture of 13H+13L grew to higher volumes (many ulcerating the skin -3 out of 5 mice-) when left untreated, upper panel. Also, within the treated mice (lower panel), the low-heteroplasmy tumors were less affected by decitabine than the high heteroplasmy ones, *p<0.05. One-tailed, unpaired Student´s t-test. **S7C.** mtDNA methylation assessment using Nanopore sequencing technology. Coverage of the whole mitochondrial genome was satisfactory and showed low methylation values that were similar in all four conditions. No significant differences were observed, however, paradoxically the 13H-dec condition showed higher trend in methylation values than its untreated counterpart. N= 3 tumors from each condition: 13H, 13H-dec, 13L, 13L.dec. **S7D.** Heteroplasmy assessment through Nanopore sequencing. Base call counts at position m.13513 are available in Supplementary file 2. Heteroplasmy was calculated as ´A´ counts/(´A´counts+´G´ counts). N= 3 tumors from each condition: 13H, 13H-dec, 13L, 13L.dec.

REFERENCES

1. Gorman, G. S. *et al.* Prevalence of nuclear and mitochondrial DNA mutations related to adult mitochondrial disease. *Ann Neurol* **77**, 753–759 (2015).

2. Thorburn, D. R. Mitochondrial disorders: Prevalence, myths and advances. *J Inherit Metab Dis* **27**, 349–362 (2004).

3. Schaefer, A. M. *et al.* Prevalence of mitochondrial DNA disease in adults. *Ann Neurol* **63**, 35–39 (2008).

4. Shahryari, A. *et al.* Development and clinical translation of approved gene therapy products for genetic disorders. *Frontiers in Genetics* vol. 10 Preprint at https://doi.org/10.3389/fgene.2019.00868 (2019).

5. Sayed, N. *et al.* Gene therapy: Comprehensive overview and therapeutic applications. *Life Sci* **294**, (2022).

6. Elangkovan, N. & Dickson, G. Gene Therapy for Duchenne Muscular Dystrophy. *J Neuromuscul Dis* **8**, S303 (2021).

7. Rossoll, W. & Singh, R. N. Commentary: Current Status of Gene Therapy for Spinal Muscular Atrophy. *Front Cell Neurosci* **16**, 930–940 (2022).

8. Gammage, P. A., Moraes, C. T. & Minczuk, M. Mitochondrial Genome Engineering: The Revolution May Not Be CRISPR-Ized. *Trends in Genetics* 101–110 (2017) doi:10.1016/j.tig.2017.11.001.

9. Schmiderer, L., Yudovich, D., Oburoglu, L., Hjort, M. & Larsson, J. Site-specific CRISPR-based mitochondrial DNA manipulation is limited by gRNA import. *Sci Rep* **12**, (2022).

10. Moraes, C. T. Tools for editing the mammalian mitochondrial genome. *Hum Mol Genet* **33**, R92–R99 (2024).

11. Mok, B. Y. *et al.* A bacterial cytidine deaminase toxin enables CRISPR-free mitochondrial base editing. (2020).

12. DiMauro, S. & Moraes, C. T. Mitochondrial encephalomyopathies. *Arch Neurol* **50**, 1197–208 (1993).

13. Srivastava, S. & Moraes, C. T. Manipulating mitochondrial DNA heteroplasmy by a mitochondrially targeted restriction endonuclease. *Hum Mol Genet* **10**, 3093–9 (2001).

14. Gammage, P. A., Rorbach, J., Vincent, A. I., Rebar, E. J. & Minczuk, M. Mitochondrially targeted ZFNs for selective degradation of pathogenic mitochondrial genomes bearing large-scale deletions or point mutations. *EMBO Mol Med* **6**, 458–466 (2014).

15. Bacman, S. R., Williams, S. L., Pinto, M., Peralta, S. & Moraes, C. T. Specific elimination of mutant mitochondrial genomes in patient-derived cells by mitoTALENs. *Nat Med* **19**, 1111–3 (2013).

16. Shoop, W. K. *et al.* Efficient elimination of MELAS-associated m.3243G mutant mitochondrial DNA by an engineered mitoARCUS nuclease. *Nat Metab* **5**, 2169–2183 (2023).

17. Falabella, M., Minczuk, M., Hanna, M. G., Viscomi, C. & Pitceathly, R. D. S. Gene therapy for primary mitochondrial diseases: experimental advances and clinical challenges. *Nat Rev Neurol* **18**, 689–698 (2022).

18. Zhou, W. *et al.* Repeated PM2.5 exposure inhibits BEAS-2B cell P53 expression through ROS-Akt-DNMT3B pathway-mediated promoter hypermethylation. *Oncotarget* **7**, 20691–20703 (2016).

19. Peng, L. *et al.* SIRT1 deacetylates the DNA methyltransferase 1 (DNMT1) protein and alters its activities. *Mol Cell Biol* **31**, 4720–34 (2011).

20. Kreuz, S. & Fischle, W. Oxidative stress signaling to chromatin in health and disease. *Epigenomics* **8**, 843–62 (2016).

21. Picard, M. *et al.* Progressive increase in mtDNA 3243A>G heteroplasmy causes abrupt transcriptional reprogramming. *Proc Natl Acad Sci U S A* **111**, E4033–E4042 (2014).

22. Kopinski, P. K. *et al.* Regulation of nuclear epigenome by mitochondrial DNA heteroplasmy. *Proceedings of the National Academy of Sciences* **116**, 16028–16035 (2019).

23. Mayorga, L. *et al.* Mitochondrial stress triggers a pro-survival response through epigenetic modifications of nuclear DNA. *Cellular and Molecular Life Sciences* **76**, 1397–1417 (2019).

24. Gawlitza, A. L. *et al.* 5-Azacytidine modulates CpG methylation levels of EZH2 and NOTCH1 in myelodysplastic syndromes. *J Cancer Res Clin Oncol* (2019) doi:10.1007/s00432-019-03016-9.

25. Christman, J. K. 5-Azacytidine and 5-aza-2′-deoxycytidine as inhibitors of DNA methylation: Mechanistic studies and their implications for cancer therapy. *Oncogene* vol. 21 5483–5495 Preprint at https://doi.org/10.1038/sj.onc.1205699 (2002).

26. Bacman, S. R., Nissanka, N. & Moraes, C. T. Cybrid technology. *Methods Cell Biol* **155**, 415–439 (2020).

27. Hashimoto, M. *et al.* MitoTALEN: A General Approach to Reduce Mutant mtDNA Loads and Restore Oxidative Phosphorylation Function in Mitochondrial Diseases. *Molecular Therapy* **23**, 1592–1599 (2015).

28. Shanske, S. *et al.* The G13513A mutation in the ND5 gene of mitochondrial DNA as a common cause of MELAS or Leigh syndrome: Evidence from 12 cases. *Arch Neurol* **65**, 368–372 (2008).

29. Wang, K., Yan, C. Z., Wang, G. X., Jiao, J. S. & Jin, M. [Mitochondrial ND5 as the causative gene of Leight syndrome]. *Zhonghua Yi Xue Yi Chuan Xue Za Zhi* **27**, 616–619 (2010).

30. Wang, W. *et al.* A different pattern of clinical, muscle pathology and brain MRI findings in MELAS with mt-ND variants. *Ann Clin Transl Neurol* **10**, 1035–1045 (2023).

31. Silvestri, G. *et al.* Clinical features associated with the A-->G transition at nucleotide 8344 of mtDNA (‘MERRF mutation’). *Neurology* **43**, 1200–1206 (1993).

32. Shoffner, J. M. *et al.* Myoclonic epilepsy and ragged-red fiber disease (MERRF) is associated with a mitochondrial DNA tRNA(Lys) mutation. *Cell* **61**, 931–937 (1990).

33. Kauppila, J. H. K. *et al.* A Phenotype-Driven Approach to Generate Mouse Models with Pathogenic mtDNA Mutations Causing Mitochondrial Disease. *Cell Rep* **16**, 2980–2990 (2016).

34. Lochmüller, H., Johns, T. & Shoubridge, E. A. Expression of the E6 and E7 genes of human papillomavirus (HPV16) extends the life span of human myoblasts. *Exp Cell Res* **248**, 186–193 (1999).

35. Nygren, A. O. H. *et al.* Methylation-Specific MLPA (MS-MLPA): Simultaneous detection of CpG methylation and copy number changes of up to 40 sequences. *Nucleic Acids Res* **33**, 1–9 (2005).

36. Pidsley, R. *et al.* Critical evaluation of the Illumina MethylationEPIC BeadChip microarray for whole-genome DNA methylation profiling. *Genome Biol* **17**, (2016).

37. Zhou, Y. *et al.* Metascape provides a biologist-oriented resource for the analysis of systems-level datasets. *Nat Commun* **10**, (2019).

38. Clarke, J. *et al.* Continuous base identification for single-molecule nanopore DNA sequencing. *Nature Nanotechnology 2009 4:4* **4**, 265–270 (2009).

39. Su, S. *et al.* NanoMethViz: An R/Bioconductor package for visualizing long-read methylation data. *PLoS Comput Biol* **17**, (2021).

40. Tan, B., Xiao, H., Li, F., Zeng, L. & Yin, Y. The profiles of mitochondrial respiration and glycolysis using extracellular flux analysis in porcine enterocyte IPEC-J2. *Animal Nutrition* **1**, 239–243 (2015).

41. Babicki, S. *et al.* Heatmapper: web-enabled heat mapping for all. *Nucleic Acids Res* **44**, W147–W153 (2016).

42. Sudo, A., Honzawa, S., Nonaka, I. & Goto, Y. I. Leigh syndrome caused by mitochondrial DNA G13513A mutation: Frequency and clinical features in Japan. *J Hum Genet* **49**, 92–96 (2004).

43. Shanske, A. L., Shanske, S. & DiMauro, S. The other human genome. *Arch Pediatr Adolesc Med* **155**, 1210–1216 (2001).

44. Andreeva, N. A., Murakhovskaya, Y. K., Tsygankova, P. G., Krilova, T. D. & Sheremet, N. L. [Leber's hereditary optic neuropathy clinical features in patients with mitochondrial DNA m.13513G>A candidate mutation]. *Vestn Oftalmol* **138**, 208–214 (2022).

45. Zeviani, M. *et al.* Rapid detection of the A→G((8344)) mutation of mtDNA in Italian families with myoclonus epilepsy and ragged-red fibers (MERRF). *Am J Hum Genet* **48**, 203–211 (1991).

46. Moslemi, A. R., Tulinius, M., Holme, E. & Oldfors, A. Threshold expression of the tRNA(Lys) A8344G mutation in single muscle fibres. *Neuromuscul Disord* **8**, 345–349 (1998).

47. Finsterer, J. Phenotypic Heterogeneity of the Mitochondrial DNA Variant m.13513 G□>□A. *J Pediatr Genet* **13**, 253 (2023).

48. Andreeva, N. A., Murakhovskaya, Y. K., Tsygankova, P. G., Krilova, T. D. & Sheremet, N. L. [Leber's hereditary optic neuropathy clinical features in patients with mitochondrial DNA m.13513G>A candidate mutation]. *Vestn Oftalmol* **138**, 208–214 (2022).

49. Buyru, N., Altinisik, J., Ozdemir, F., Demokan, S. & Dalay, N. Methylation profiles in breast cancer. *Cancer Invest* **27**, 307–312 (2009).

50. Maleva Kostovska, I. *et al.* TIMP3 Promoter Methylation Represents an Epigenetic Marker of BRCA1ness Breast Cancer Tumours. *Pathol Oncol Res* **24**, 937–940 (2018).

51. Furlan, D. *et al.* Diagnostic utility of MS-MLPA in DNA methylation profiling of adenocarcinomas and neuroendocrine carcinomas of the colon-rectum. *Virchows Arch* **462**, 47–56 (2013).

52. Davletgildeeva, A. T. & Kuznetsov, N. A. The Role of DNMT Methyltransferases and TET Dioxygenases in the Maintenance of the DNA Methylation Level. *Biomolecules* **14**, 1117 (2024).

53. Deaton, A. M. & Bird, A. CpG islands and the regulation of transcription. *Genes Dev* **25**, 1010–1022 (2011).

54. Adrian, B. Genetic determinants of the epigenome in development and cancer. *Swiss Med Wkly* **147**, (2017).

55. Razin, A. & Riggs, A. D. DNA methylation and gene function. *Science* **210**, 604–610 (1980).

56. Esteller, M. *et al.* The Epigenetic Hallmarks of Cancer. *Cancer Discov* **14**, 1783–1809 (2024).

57. Stoccoro, A. & Coppedè, F. Mitochondrial dna methylation and human diseases. *International Journal of Molecular Sciences* vol. 22 Preprint at https://doi.org/10.3390/ijms22094594 (2021).

58. Tong, H. *et al.* Methylation of mitochondrial DNA displacement loop region regulates mitochondrial copy number in colorectal cancer. *Mol Med Rep* **16**, 5347–5353 (2017).

59. Carvalho, A. L. *et al.* Evaluation of promoter hypermethylation detection in body fluids as a screening/diagnosis tool for head and neck squamous cell carcinoma. *Clin Cancer Res* **14**, 97–107 (2008).

60. Epigenetic patterns in the progression of esophageal adenocarcinoma - PubMed. https://pubmed.ncbi.nlm.nih.gov/11309301/.

61. Reinert, T. *et al.* Clinical implication of low estrogen receptor (ER-low) expression in breast cancer. *Front Endocrinol (Lausanne)* **13**, (2022).

62. Osuna, M. A. L. *et al.* Activation of estrogen receptor alpha by decitabine inhibits osteosarcoma growth and metastasis. *Cancer Res* **79**, 1054–1068 (2019).

63. Kärppä, M. *et al.* Spectrum of myopathic findings in 50 patients with the 3243A>G mutation in mitochondrial DNA. *Brain* **128**, 1861–1869 (2005).

64. Achinger-Kawecka, J. *et al.* The potential of epigenetic therapy to target the 3D epigenome in endocrine-resistant breast cancer. *Nature Structural & Molecular Biology 2024 31:3* **31**, 498–512 (2024).

65. Gutierrez, W. R. *et al.* Augmenting chemotherapy with low-dose decitabine through an immune-independent mechanism. *JCI Insight* **7**, (2022).

66. Aminuddin, A., Ng, P. Y., Leong, C. O. & Chua, E. W. Mitochondrial DNA alterations may influence the cisplatin responsiveness of oral squamous cell carcinoma. *Sci Rep* **10**, (2020).

67. Morris, M. J. *et al.* Reduced nuclear DNA methylation and mitochondrial transcript changes in adenomas do not associate with mtDNA methylation. *Biomark Res* **6**, (2018).

68. Matilainen, O., Quirós, P. M. & Auwerx, J. Mitochondria and Epigenetics – Crosstalk in Homeostasis and Stress. *Trends in Cell Biology* vol. 27 453–463 Preprint at https://doi.org/10.1016/j.tcb.2017.02.004 (2017).

69. Dey, R. & Moraes, C. T. Lack of oxidative phosphorylation and low mitochondrial membrane potential decrease susceptibility to apoptosis and do not modulate the protective effect of Bcl-x(L) in osteosarcoma cells. *J Biol Chem* **275**, 7087–7094 (2000).

70. Bayona-Bafaluy, M. P., Blits, B., Battersby, B. J., Shoubridge, E. A. & Moraes, C. T. Rapid directional shift of mitochondrial DNA heteroplasmy in animal tissues by a mitochondrially targeted restriction endonuclease. *Proc Natl Acad Sci U S A* **102**, 14392–7 (2005).

71. Foulks, J. M. *et al.* Epigenetic Drug Discovery:Targeting DNA Methyltransferases. *J Biomol Screen* **17**, 2–17 (2012).

72. Christman, J. K. 5-Azacytidine and 5-aza-2′-deoxycytidine as inhibitors of DNA methylation: Mechanistic studies and their implications for cancer therapy. *Oncogene* **21**, 5483–5495 (2002).

73. Stresemann, C. & Lyko, F. Modes of action of the DNA methyltransferase inhibitors azacytidine and decitabine. *Int J Cancer* **123**, 8–13 (2008).

74. Christman, J. K. 5-Azacytidine and 5-aza-2’-deoxycytidine as inhibitors of DNA methylation: mechanistic studies and their implications for cancer therapy. *Oncogene* **21**, 5483–5495 (2002).

75. Khotina, V. A., Vinokurov, A. Y., Bagheri Ekta, M., Sukhorukov, V. N. & Orekhov, A. N. Creation of Mitochondrial Disease Models Using Mitochondrial DNA Editing. *Biomedicines* **11**, (2023).

76. Guo, J. *et al.* Precision modeling of mitochondrial diseases in zebrafish via DdCBE-mediated mtDNA base editing. *Cell Discov* **7**, (2021).

77. Lee, S. *et al.* Enhanced mitochondrial DNA editing in mice using nuclear-exported TALE-linked deaminases and nucleases. *Genome Biol* **23**, (2022).

78. Sabharwal, A. *et al.* The FusX TALE Base Editor (FusXTBE) for Rapid Mitochondrial DNA Programming of Human Cells In Vitro and Zebrafish Disease Models In Vivo. *CRISPR J* **4**, 799–821 (2021).

79. Barcelos, I., Shadiack, E., Ganetzky, R. D. & Falk, M. J. Mitochondrial medicine therapies: rationale, evidence, and dosing guidelines. *Curr Opin Pediatr* **32**, 707–718 (2020).

80. Jiang, Q. *et al.* Mitochondria-Targeted Antioxidants: A Step towards Disease Treatment. *Oxid Med Cell Longev* **2020**, 8837893 (2020).

81. Kadi, F. *et al.* The effects of heavy resistance training and detraining on satellite cells in human skeletal muscles. *J Physiol* **558**, 1005–1012 (2004).

82. Vidman, S., Ma, Y. H. E., Fullenkamp, N. & Plant, G. W. Human induced pluripotent stem cell-derived therapies for regeneration after central nervous system injury. *Neural Regen Res* **20**, 3063–3075 (2025).

83. Fine, B. & Vunjak-Novakovic, G. Heart regeneration in mouse and human: A bioengineering perspective. *Curr Opin Physiol* **14**, 56–63 (2020).

84. Murphy, J. L. *et al.* Resistance training in patients with single, large-scale deletions of mitochondrial DNA. *Brain* **131**, 2832–2840 (2008).

85. Luo, Y., Ma, J. & Lu, W. The Significance of Mitochondrial Dysfunction in Cancer. *Int J Mol Sci* **21**, 5598 (2020).